Ozone pollution episodes and PBL height variation in the NYC urban and coastal areas during LISTOS 2019

Yonghua Wu [1, 2*], Kaihui Zhao [3], Xinrong Ren [4, 5], Russell R. Dickerson [5], Jianping Huang [6], Margaret J. Schwab [7], Phillip R. Stratton [5], Hannah Daley [5], Dingdong Li [1], Fred Moshary [1, 2]

[1] Optical Remote Sensing Lab, City College of New York (CCNY), New York, NY 10031, USA, [*] Email: yhwu@ccny.cuny.edu

[2] NOAA–Cooperative Science Center for Earth System Sciences and Remote Sensing Technologies (CESSRST), NY 10031, USA

[3] Yunnan Key Laboratory of Meteorological Disasters and Climate Resources in the Greater Mekong Sub-region, Yunnan University, Kunming, 650091, China

[4] Air Resources Laboratory, National Oceanic and Atmospheric Administration (NOAA), College Park 20742, MD, USA

[5] Department of Atmospheric and Oceanic Science, University of Maryland, College Park (UMD), MD 20742, USA

[6] NOAA/NCEP/ Environmental Modeling Center and Lynker, College Park, MD 20740, USA

[7] Atmospheric Sciences Research Center, University at Albany, State University of New York, Albany, NY, USA

Abstract In summer, frequent ozone (O_3) episodes occur in New York City (NYC) and coastal areas along Long Island Sound (LIS) due to complex interplay of urban pollutants transport, land-sea breezes, and chemistry. The Long Island Sound Tropospheric Ozone Study (LISTOS) was carried out to address this issue; here we present an integrated analysis of the diurnal variation of planetary-boundary-layer height (PBLH) and O_3 in the NYC urban and coastal area during LISTOS in summer 2019. A persistent O_3 episode (July 28-31, 2019) is investigated which shows much higher O_3 (90-120 ppb with 5-min average maximum) along the North-shore of Long Island (NLI) than the NYC urban and South-shore of Long Island (SLI). We evaluate the PBLH estimate with a multi-platform observation in the complex coastal environment, and compare the PBLH diurnal variation in the NYC urban to coastal areas. The results indicate lower PBLH in the mid-morning and noon in the NLI than the NYC urban area. With the simultaneously measured O_3 and PBLH, the integrated O_3 content or total content in the PBL defined as the O_3 concentrations multiplying PBLH show good consistency in the urban and NLI coast at noon on July 28-29, 2019. A dense O_3 plume, rich in CO, aerosols, black carbon, HCHO and NOx appeared in the PBL as detected from the UMD Cessna research aircraft, satellite TROPOMI and ozonesonde; their coincidently large values imply the combined impacts of urban plumes transport, lower PBLH and land-sea breezes in the NLI area. Finally, we evaluated the forecast of O_3 and PBLH from the NOAA NAM-CMAQ (12 km grid) and WRF-Chem (1.3 km grid) models with the observations. Both models show good agreement with the observations at the NYC urban site; but at the NLI coastal site, the NAM-CMAQ model forecast indicates a timing bias for the maximum O_3 at noon. These results provide insight into the impacts of the sea breeze and urban heat island on air quality.

Keywords: Ozone, PBL, Transport, Sea breezes

1. Introduction

Ozone (O_3) exceedances of National Ambient Air Quality Standard (NAAQS, 70 ppb daily maximum 8-hour average ozone, DM8AO) frequently occur during summer in New York City (NYC) and its downwind coastal areas in Long Island and Connecticut or Long Island Sound (Miller, 2017; Karambelas, 2020). Such high O_3 episodes are generally related to complex interaction of urban emissions and pollutants, photochemical transformation, transport, and land-sea breezes effects (Karambelas, 2020). To understand high O_3 formation processes, the Long Island Sound Tropospheric Ozone Study (LISTOS) campaign was launched in summer 2018 and 2019 (https://www.nescaum.org/documents/listos). The measurements were made from the land sites, research aircrafts and marine vessels, and space in Long Island Sound (LIS) where a land–sea breeze feature can lead to high O_3 concentrations along the shoreline of Connecticut and New York State (see more logistic information in Karambelas, 2020).

Planetary boundary layer height (PBLH), dynamics and structure often affect the pollutants dispersion and transport. Angevine et al. (2004) indicate the coastal boundary layer influence on pollutant transport in New England during the New England Air Quality Study (NEAQS). The lack of vertical mixing and deposition over the water and the sea breezes could affect the air pollutant transport levels in the coastal area over the Galveston Bay in Houston area (Angevine et al., 2008). The shallow PBLH can keep the morning emissions and pollutants confined at near-surface. In addition, the land-water breezes have been investigated to understand O_3 accumulation in the coastal areas (Caicedo et al., 2019 and 2021; Day et al., 2010; Finardi et al., 2018; Goldberg et al., 2014; Han et al., 2022; Loughner et al., 2011, 2014; Stuffer et al., 2015; Vermeuel, et al., 2019; Zhang et al., 2020). Zhang et al (2020) show a sharp gradient of O_3 at and near the land-water interface in Long Island using a mobile measurement during LISTOS 2018, which is attributed to the sea-breezes in the Northern Long Island. Han et al. (2022) analyzed sea breezes life cycle in and around NYC that made dramatic impacts ozone patterns in NYC region. Caicedo et al. (2019 and 2021) showed that the different bay-breezes in the horizontal and vertical evolution of wind affected the O_3 vertical structure during the Ozone Water-Land Environmental Transition Study Phase-2 (OWLETS-2) campaign (Sullivan et al., 2019). On the other hand, Tao et al. (2022) compared the PBLH on five O_3 exceedances and five nonexceedance days during the LISTOS campaign in NYC using the WRF-CMAQ simulation product (1.33 km grid resolution), and the results indicated lower PBLH on O_3-exceedance days at noon time with a regional mean decrease of 0.22-0.24 km.

According to Stull (2012), a convective boundary layer (CBL) that occurs in the daytime is usually referred to as a mixing layer (ML); under this situation, the mixing layer height (MLH) is equivalent to PBLH (the MLH and PBLH may be used in the content of this paper). Ceilometer and Coherent Doppler Wind lidar are extensively deployed to make continuous observation of PBLH or MLH and dynamics (Caicedo et al., 2020, Haeffelin et al., 2012, Schween et al., 2014, Tucker et al., 2009, Zhang et al., 2022). The MLH can be estimated from the ceilometer-measured aerosol profile through locating sharp gradient of attenuated backscatter distribution. However, large uncertainty stems from aloft aerosol layers, residual aerosols and low-level clouds, thus a quality control and quality assurance (QA/QC) process is often required to remove those outliers for the MLH estimate (Caicedo et al., 2020, Haeffelin et al., 2012; Li et al., 2022). Particularly for transported urban and wildfire smoke plume to the coastal area, the gradient at the aloft-layer top may not represent local MLH. On the other hand, Coherent Doppler Wind Lidar (CDWL) is widely used to measure the 3D winds in the PBL. Most commercial CDWL is operated at around 1.5 μm wavelength and its signal-to-noises (SNR) or carrier-to-noise ratios (CNR) depend on aerosol concentrations. Vertical motions in the PBL can be quantified from vertical

stares (non-scanning mode) performed by a Doppler wind lidar, and variance of vertical velocity generally represents vertical mixing or turbulence intensity thereby indicating convective boundary layer height (CBLH) or MLH (Tucker et al., 2009). However, this method requires an empirical threshold for the MLH estimate and this threshold may vary with the vertical turbulent intensity and geo-location, and it may not work properly under stable boundary layer (SBL) condition due to weak turbulence, particularly over the water and coastal area (Schween et al., 2014, Tucker et al., 2009). Alternatively, a gradient method for CNR profile is used for the SBL height (SBLH) estimate but suffers similar issue as the ceilometer method due to aloft aerosol layer and low CNR issues. On the other hand, a gradient method on the horizontal wind profile may work for the SBLH estimate (Tucker et al., 2009). Another issue is that the ceilometer and wind lidar generally collect reliable atmospheric returns above 100-m altitude; thus shallow SBLH lower than 100-m is difficult to detect from their measurements. In the meantime, meteorology-based methods (e.g., potential temperature gradient or Richardson number (R_i)) from radiosonde measurements can also be used to determine the PBLH though such observations are routinely made twice per day (00:00 and 12:00 UTC) at national weather station. Thus, it is important to evaluate PBLH or MLH estimate among these different methods in the coastal area while the LISTOS campaign provides an opportunity for this research purpose.

In addition, air quality models such as the Community Multiscale Air Quality modeling (CMAQ) have been extensively used to predict O_3 and address high O_3 events (Dreessen et al., 2016), but there are potentially large uncertainties in coastal areas due to complex meteorological effects over the land-water interface and limited spatial resolution (Abdi‐Oskouei et al., 2020; Ma et al., 2021; Torres-Vazquez1 et al., 2022; Bernier et al., 2022). For instance, using the WRF-Chem (4 km horizontal or grid resolution) over the Lake Michigan Ozone Study 2017 (LMOS), Abdi‐Oskouei et al. (2020) indicated that the model skill on Lake breeze was inconsistent depending on site and day; for some sites or cases, hourly peak O_3 from WRF-Chem could be underestimated and the bias might be attributed to transport and lake breeze errors. They also found that increases in hydrocarbon emissions could increase O_3 production by the model and reduce the mode error over the Lake Michigan. Previous studies (Loughner et al., 2011, 2014; Goldberg et al., 2014; Caicedo et al., 2019) indicate that the timing and strength of the sea-breeze are key for correctly simulating pollution events whereas it is a challenge to model simulation of sea-breezes as they are sensitive to the land-water surface contrast, spatially coarse initial conditions and horizontal resolution. It was found that the initial analysis and land surface behavior for the WRF modeling were the important items in getting good simulations of PBLH and O_3 (Angevine et al., 2008). In addition, Torres-Vazquez1 (2022) evaluated the WRF-CMAQ simulation performance of the meteorology and O_3 for the LISTOS 2018, and the two cases studies suggest that higher spatial resolution (1.3 km grid) improve surface meteorology simulation throughout the whole summer; and the sound breezes and low-level jets played an important role in the transport of urban emissions and pollutants to marine boundary layer in LIS and advection to the CT coast. In addition, in the NYC urban area anthropogenic volatile chemical products (VCPs) and volatile organic compounds (VOCs) can make a great contribution to high O_3 production (Coggan et al., 2021; Ring et al., 2023), thus becoming important for the models to achieve accurate predictions.

Synergistic and collaborative measurements and model studies have been performed in LISTOS campaigns for understanding high O_3 formation and transport mechanisms. One of the major concerns is how the urban plume transport, PBL dynamics, and land-sea breeze affect near-surface O_3 during the O_3

episodes period in the coastal area. The scopes of this study include: 1) evaluating PBLH estimate among the different methods/instruments, and comparing the PBLH dynamics in the NYC urban and coastal area; 2) analyzing high O_3 formation relevant to vertical mixing, PBLH, sea breezes and urban plume transport in the coastal area; 3) assessing the model forecast of O_3 and PBLH by the NOAA NAM-CMAQ and WRF-Chem at the NYC urban and coastal sites. This paper is organized as follows, Section-2 gives the observation and methodology; Section-3 presents the results and discussions, with the conclusions following in Section 4.

2. Observation and Methodology

2.1 Ground-based observations

At the City College of New York (CCNY) site (40.820° N, 73.949° W), there are a suite of remote sensing and in-situ instruments for air quality and meteorological observations, which include a ceilometer, a 3-wavelength elastic-Raman scattering lidar, a microwave radiometer (Radiometric MP-3000A), a Cimel sun/sky radiometer in part of AERONET (Aerosol Robotic Network), a coherent Doppler wind lidar (Leosphere Windcube 200S), in-situ samplers for O_3, NO_2 and aerosol size distribution and a weather station. The observations are mostly operated with 1-min average. Meanwhile, a surface air quality monitoring station (AQS) is operated by New York State Department of Environmental Conservation (NYSDEC) at CCNY campus for O_3, CO and $PM_{2.5}$ measurement. **Figure 1** and Table-1 show the geolocations of CCNY-site and other ground sites used in this study.

At CCNY, a Lufft ceilometer (CHM15K) measures aerosol backscatter at a laser wavelength of 1064 nm with a vertical range resolution of 15-m and time resolution of 15-second. It makes fully automatic 24-hr/7-day observations under all-weather conditions and provides attenuated backscatter coefficient profiles that can be used to determine aerosol layer height (ALH) and cloud base height (CBH). The valid return signals start from around 150~180 m altitude due to inherent geometric overlap function between the transmitter and receiver (Li et al., 2021). In this study, we use a wavelet transform method to determine the PBLH, and a quality control algorithm is performed which includes cloud screening, temporal continuity, and screening of an aloft or residual layer during the night and early-morning (Gan et al., 2011, Li et al., 2022). A residual-layer-height (RLH) can be estimated from the second sharp gradient of aerosol profile in the early morning. In addition, the CCNY elastic-Raman lidar transmits three wavelengths (1064-, 532- and 355-nm) with a flash lamp-pumped Nd: YAG laser at a repetition rate of 30 Hz (Spectra-physics Quanta-Ray PRO-320) (Wu et al., 2009). A receiver telescope (Ø50-cm) collects three elastic scattering and two Raman-scattering returns by nitrogen and water vapor molecules excited by the 355-nm laser output. It is generally operated during daytime on weekdays with an observer due to eye-safety concerns in the NYC urban area. The strong signal-to-noise ratios (SNR) of this lidar allow us to measure aloft aerosol plumes and retrieve aerosol extinction and backscatter profile; thus one can obtain PBLH and aloft aerosol plumes optical properties (Gan et al., 2011, Wu et al., 2012, 2019 and 2021).

In addition, two sets of ceilometers (Vaisala CL51 and CL31) and O_3 monitors (2B Tech model 202/205) are deployed at the North-shore (Eatons Neck, 40.954176°N, 73.398471°W) and South-shore (Fire Island, 40.625282°N, 73.257897°W) of Long Island during July 22-Oct.15, 2019, respectively. These two sites are close to the waterfront (a few tens meters distance). The attenuated backscatter profiles at the wavelength of 905-nm are collected with a range resolution of 10-m and time resolution of

16-second. We estimate the PBLH or MLH using a wavelet transform analysis and quality assurance method with a 10-min average (Li et al., 2022). Meanwhile, near-surface O_3 data are collected with 5-min average. We validated the O_3 data of the 2B-Tech monitors with the NYSDEC operated sampler before we deployed them to the coastal sites; the data were simultaneously collected at the NYSDEC AQS at CCNY during July 9-14, 2019, and the results indicate strong correlation with correlation coefficient R>0.99 and a linear slope of 1.02~1.03 (See **Fig. S1(a)-(b) in Supporting Document**). We also validated our NO_2 data by comparing them to the NYSDEC monitor data. The results indicate good correlation with R=0.995, linear regression slope=1.07 and intercept value of 0.36 (**See Fig.S1(c)-(d) in Supporting Document)**. Therefore, near-surface O_3, PBLH, low-altitude aerosol plumes and cloud height can be simultaneously measured in the NYC urban (CCNY) and its downwind coastal area in Long Island (Eatons Neck and Fire Island). In addition, a few other AQS for O_3 measurements are operated by NYSDEC at the coastal area, e.g., Flax Pond (O_3, NO_2 and NO_y), Riverhead (O_3) at the North-Shore of Long Island (NLI), Babylon (O_3) near to South Long Island (SLI). Further details about these sites can be found at the website (http://www.dec.ny.gov/chemical/8406.html). Fig.1 and Table-1 give the site locations, coordinates and data used in this study.

As part of the NYS-Mesonet (Brotzge et al., 2020, Shrestha et al., 2021), Coherent Doppler Wind Lidars (Leosphere WindCube 100s) are deployed to measure wind profiles in Bronx (Lehman College, 40.87248° N, 73. 8935° W, 59.3 m ASL, 7.5 km away from CCNY, urban), Stony Brook (40.9196°N, -73.1333°W, 55.1 m ASL) near the North-shore of Long Island, and Wantagh (40.6503°N, 73.5054°W, 18.25 m ASL) at the South-shore Long Island, respectively (See Fig.1 for their location). The wind lidar emits the eye-safe laser beams at the wavelength 1.54 μm and a repetition rate of 10 kHz. It uses a vertically-pointing beam to measure vertical wind velocity, and a Doppler Beam Swinging (DBS) scan mode (elevation angle 75 degrees) to obtain horizontal wind velocity and direction. All data are collected, quality-controlled, and archived (Brotzge et al., 2020, Shrestha et al., 2021). It provides 24-hr/7-day wind profile measurements under all weather conditions. The constructional 3D-wind products have a range-gate spacing of 25-50 m and a time resolution of 5~20 seconds. In this study, we estimate the PBLH or MLH using the variance of vertical velocity with a threshold method (e.g., 0.1-0.15 m/s^2) during the convective boundary layer (CBL) period (Tucker et al., 2019, Wu et al., 2019). Meanwhile, during the stable boundary layer (SBL) period in the morning and night, the PBLH is calculated with the vertical gradient of horizontal wind with a threshold (0.02-0.04 per second) (Tucker et al., 2019, Dai et al., 2014). The PBLHs from the wind lidar and ceilometer estimates are evaluated with the meteorological profile-based method (e.g., potential temperature) measured by the radiosonde launched at a National Weather Service station at Upton (OKX, 40.86° N, 72.86° W, 20-m ASL) and the ozonesonde at Stony Brook.

The ozonesondes are launched at Stony Brook (SBK) during LISTOS 2019 and at the Flax Pond Marine Laboratory (40.9615° N, 73.13872° W) during the LISTOS 2018 campaign (Couillard et al., 2021), both sites are located near the North shore of Long Island. Vaisala radiosondes (Vaisala RS41-SGP) with an En-Sci Electrochemical Cell ozonesonde (En-Sci) provided data at 1-sec intervals, with an uncertainty of 5-10% on the ozone mixing ratio in the troposphere and ~5% in stratosphere (Witte et al., 2018). Vertical profiles of O_3 and meteorological parameters (temperature, pressure, wind, relative humidity-RH) are recorded. Nearby Flax Pond (surface O_3 site) and Stony Brook (wind-lidar and ozonesonde site in this study), the radiosondes are routinely launched at OKX site twice per day (12:00

UTC and 24:00 UTC) for profiling temperature, pressure, RH and winds. During the CBL period, the PBLH is determined from the sharp increase of virtual potential temperature (Seidel et al., 2010; Dai et al., 2014). During the SBL period, the PBLH is estimated from the inversion temperature height. The distance is about 22 km between the radiosonde-OKX and wind-lidar site (SBK), 4.8 km between surface O_3 site (Flax Pond) and wind-lidar site (SBK), 20-km between the ceilometer-site (Eatons Neck) and wind-lidar site (SBK), respectively. Therefore, with the distances noted, we compare the PBLH bias among the wind lidar, ceilometer and radiosonde measurements. All ground sites used in this study are shown in Fig.1 and Tab.1.

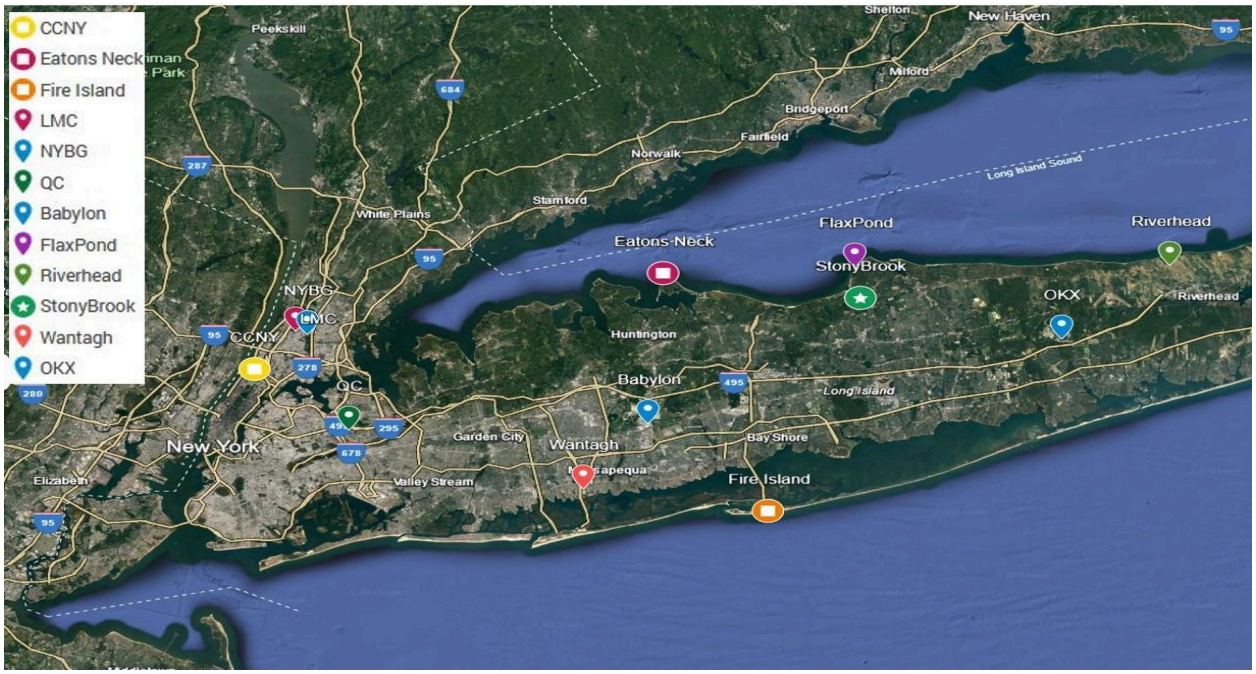

Fig.1. Ground sites used in this study (See Table-1 for their coordinates and observations).

Table-1. Ground site location and the data used in this study*

Site-name	Latitude	Longitude	Data used		Operator, landmark
	(north, deg)	(west, deg)	Surface	Profile	
CCNY	40.821	-73.949	O_3,NO_2,T, Wind	Aerosol	CCNY+NYSDEC, Urban
Eatons Neck	40.954	-73.398	O_3	Aerosol	CCNY, Coast, NLI
Fire Island	40.625	-73.258	O_3	Aerosol	CCNY, Coast, SLI
NYBG	40.868	-73.878	O_3		NYSDEC-AQS, Urban
QC	40.736	-73.822	O_3,NO_2		NYSDEC-AQS, Urban
Babylon	40.745	-73.419	O_3		NYSDEC-AQS, Coast
Riverhead	40.961	-72.712	O_3		NYSDEC-AQS, Coast
Flax Pond	40.961	-73.138	O_3, NO_2		NYSDEC+ASRC, Coast
LMC(Bronx)	40.873	-73.894		Wind	NYS-Mesonet, Urban

Stony Brook	40.920	-73.133	T, Wind	Wind, O_3	NYS-Mesonet+ASRC
Wantagh	40.650	-73.505		Wind	NYS-Mesonet, Coast
OKX	40.860	-72.86		T, Wind	NOAA-NWS

*The acronyms in Table-1 are spelled with their full names in the contexts. See the site location in Fig.1. All sites are continuously collected the data for 24 hours/7 days except OKX-site radiosonde launch twice per day.

2.2 University of Maryland (UMD) research aircraft observations

The UMD Cessna research aircraft was deployed to measure gas compounds (O_3, CO, NOx, Formaldehyde (HCHO), CO_2, CH_4, etc.), aerosol optical properties (total scattering and absorption), black carbon (BC) and meteorological parameters during the LISTOS campaigns. This study uses the data measured in Long Island and NYC area on July 29, 2019. In particular, its simultaneous measurements of vertical profiles of aerosol, potential temperature, H_2O, and winds can be used to evaluate the PBLH estimate from the different methods; and its low-leg flight measurements can help assess spatial homogeneity of O_3 and other pollutants/parameters in the NYC and LIS region. The technical details on the instruments and observations can be found in the literatures (Taubman et al., 2004, Castellanos et al., 2011; Ren et al., 2018, 2019).

2.3 Satellite sensors for NO_2, HCHO and smoke plumes

TROPOspheric Monitoring Instrument (TROPOMI) on board the EPA Sentinel 5 Precursor (S5P) satellite was launched in October 2017 (Griffin, et al., 2019). It is a UV, visible (Vis), near-infrared, shortwave infrared backscattering sensor with an overpass time of 13:30 local solar time. Tropospheric column amounts of NO_2 and HCHO product from TROPOMI are used in this study. The Level-2 data have the spatial resolution of 7 km x 3.5 km (at nadir) during Apr.30, 2018 to Aug.6, 2019 and 3.5 km×5.5 km since Aug.6, 2019. The level-2 data product are downloaded (disc.gsfc.nasa.gov/) and selected with the quality assurance (QA>0.5).

NASA space-borne lidar CALIOP instrument on board the CALIPSO satellite platform observes global aerosol/cloud vertical distribution and provides aerosol type classification and optical properties products (Winker et al., 2009). It is a polarization-sensitive two-wavelength (532- and 1064-nm) lidar. In this study, the vertical distribution of Level-1 attenuated backscatters and the Level-2 aerosol subtypes product (Version 4.10) are used to identify aerosol plumes and their types around NYC area.

In addition, the NOAA Hazard Mapping System (HMS) was developed in 2001 by the National Environmental Satellite and Data Information Service (NESDIS) as an interactive tool to identify fires and smoke emissions over North America in an operational environment (Ruminski et al., 2006). The system utilizes two geostationary and five polar orbiting environmental satellites (https://www.ospo.noaa.gov/Products/land/hms.html). The result is a quality-controlled display of the locations of fires and significant smoke plumes. HMS has a number of detection limitations such as clouds hindering detections, no vertical structure information and no quantitative amount or density of smokes and is only available during daylight. In addition, the NOAA- HYbrid Single Particle Lagrangian Integrated Trajectory (HYSPLIT) model is used to compute air parcel trajectories and model the dispersion and the route of airborne particles (Stein et al., 2015), it can be used either in a back-trajectory mode to analyze sources or in forecast mode.

2.4 Model forecast product

The National Air Quality Forecasting Capability (NAQFC) was established by NOAA in partnership with the EPA to provide operational forecasts of O_3 and $PM_{2.5}$. The NOAA-Air Resources Laboratory (ARL) and the NCEP develop upgrades for the NAQFC forecasting system, conduct and evaluate pre-implementation testing (Lee et al., 2016; Huang et al., 2017; Campbell et al., 2022). The operational NAQFC consists of the NOAA-NCEP regional operational weather forecasting model, North America Model (NAM) and EPA-CMAQ model before 2021 while it has been upgraded with a new dynamical core known as the Finite-Volume Cubed-Sphere (FV3) in the Global Forecast System (GFS) model since summer 2021 (Campbell et al., 2022). It is designed to provide 2-day model forecasts of O_3 and $PM_{2.5}$ twice per day at the 06 and 12 UTC cycles. In this study, the operational NAQFC forecast products with spatial resolution of 12 km at the 06 UTC cycle are used. The NAQFC performs incremental tests and evaluations against the U.S. EPA AIRNow surface monitoring network. A modified version of the U. S. EPA CMAQ v5.0.2 (Foley et al., 2010), is run at 12-km horizontal grid spacing with a Lambert Conformal Conic (LCC) map projection for the product used in this study. The offline coupling between NWS/NCEP NAM meteorological model and CMAQ is achieved by two pre-processors. In addition to the coupled Nonhydrostatic Multiscale Model with Arakawa B-grid staggering (NMMB)-CMAQ system, there are other components such as an emission module and chemical lateral boundary condition builder as well as the products generating post-processing components. Emission inventories are processed by sectors where the fire sectors include prescribed burns and wildfires in the 2017 National Emission Inventory (NEI). The U.S. EPA-NEI 2014 version is processed by the interface PreMAQ for this study period. The 2006 Environment Canada National Inventory sources were used for the Canada-related region within the NAQFC domain, and the 2012 Mexico NEI non-road sources were used for Mexico parts. The emissions from wildfires, prescribed agricultural burns, and land clearing fires were computed using the dynamic fire emission modeling U.S. Forest Service BlueSky smoke emission package (O'Neill et al., 2009) and the NOAA-HMS for fire locations and strength. The latest version of the Biogenic Emission Inventory System (BEIS) v3.6.1 is used for estimating the biogenic VOC (BVOC) emissions (Campbell et al., 2022).

The NAQFC CMAQv5.0.2 follows largely the U.S. EPA Aero4 module and the related emission and removal processes found in the U.S. EPA-CMAQ version 5.0.2. Gas to particle conversion, heterogeneous reactions, depositional growth, and coagulation are included (Kelly et al., 2009). The Aero4 module simulates particle formation, condensational and coagulation growth or evaporative dissipation of existing particles due to ambient chemical, temperature and humidity conditions. The Mellor Yamada Janjic (MYJ) PBL scheme (Janjie et al., 2001) is used in this version of NAM. The detailed configuration for the NAQFC simulations can be found in Lee et al. (2016) and Huang et al. (2017).

In addition, the WRF/Chem model (version 3.9.1) is used for ground O_3 and PBLH predict in this study (Zhao et al., 2019, 2023). The grid point dimensions from the outermost to the innermost domains are 85 × 75, 76 × 70, and 70 × 61 with horizontal resolutions of 12 km, 4 km and 1.3 km, respectively. Outputs from the Whole Atmosphere Community Climate Model (WACCM) provide initial and lateral conditions of chemical species to drive the WRF/Chem simulations. This study will compare the forecast data products of surface O_3 and PBLH from NOAA NAM-CMAQ (12 km resolution) and WRF-Chem (1.3 km resolution) models to the observations in the NYC urban and coastal sites, and observe their performance in term of their different spatial resolution. The WRF/Chem model simulations provide the hindcast data after the campaign period.

The parameterization schemes used in the WRF/Chem simulations include microphysics scheme of Lin et al. (1983), Goddard shortwave radiative transfer scheme (Chou and Suarez, 1994), Yonsei University PBL scheme (Hong et al., 2006), Rapid Radiative Transfer Model longwave radiation scheme (Mlawer et al., 1997). Version 2 of the Regional Acid Deposition Model (RADM2) (Stockwell et al., 1990), and Fast-J photolysis scheme (Wild et al., 2000).

In the WRF-Chem model simulation, the Model for Ozone and Related Chemical Tracers Version 4 (MOZART-4/GEOS5) (Emmons et al., 2010) products are used to provide chemical initial and lateral conditions to the model simulations. Anthropogenic emissions from point, on-road mobile, non-road mobile, and area sources with a 4-km spatial resolution are provided by the 2014 National Emissions Inventory (NEI) developed by the U.S. Environmental Protection Agency (EPA). Hourly weekday emissions for the four major inventory components (point, on-road mobile, non-road mobile, and area) with a 4-km spatial resolution (available at ftp://aftp.fsl.noaa.gov/divisions/taq) are used in this study. The data are currently available for the contiguous 48 states of the United States, southern Canada and northern Mexico (Brioude et al., 2013; Choi and Souri, 2015). Biogenic emissions are calculated using the Model of Emissions of Gases and Aerosols from Nature v2.1 (MEGAN) (Guenther et al., 2012). The fire emissions inventory is based on the Fire Inventory from NCAR (FINN) (Wiedinmyer et al., 2011) which provides daily average of fire emissions data. More details on the model configurations and land-use categories can be found in Zhao et al. (2019 and 2023); we have evaluated the WRF-Chem model predict of surface O_3 exceedance for summer heat-wave event in NYC area (Zhao et al., 2019) and the O_3 profiles with ground observations during LISTOS 2018 (Zhao et al., 2023).

3. Results and Discussions

3.1 O_3 episode and surface meteorology

Figure 2 shows the temporal variation of ground-level O_3 and NO_2 in the NYC urban (CCNY) and coastal area (Eatons Neck and Fire Island) in Long Island during July 25-31, 2019, respectively. In Fig.2 (a), the O_3 concentrations show highest values at Eatons Neck in the NLI than other two sites on July 28-31, whereas the O_3 concentrations are higher at Fire Island on July 25-26, 2019. In particular, the near-surface O_3 show a dramatic increase from 35 ppb to 110 ppb at 8:00 am-3:00 pm (local time or EDT) and attain the maximum at 100-120 ppb on July 28-30 at Eatons Neck. However, at CCNY-site the O_3 show the maximum values of 60-70 ppb at 12:00-16:00 on July 28-29. In addition, in the night-time, the O_3 at Eatons Neck is generally higher than at CCNY with the absolute difference of around 40 ppb on July 29-30, 2019. As one of the O_3 major precursors, the NO_2 at Flax Pond (Fig.2 (b)) is much lower than at CCNY and QC sites, which indicates that the local photochemical production at the coastal site may not be a major source of the high O_3 for this event. The maximum daily 8-hour average O_3 (MD8AO) concentrations exceed 70 ppb on July 28 and 29 at Flax Pond in the North-shore of Long Island (https://www.dec.ny.gov/docs/air_pdf/2019o3ecx.pdf). As shown in Fig.2(c)-(d), the daily O_3 air quality index (AQI) indicates the unhealthy levels in the coastal area of Long Island Sound on July 28-29, 2019.

Figure 3 shows air temperature, horizontal wind speed and direction recorded at the weather station of CCNY, Stony Brook (NLI) and Fire Island (SLI) on July 25-31, 2019, respectively. A heat-wave event with the maximum temperature T_{max}> 32.2°C or 90°F was indicated at CCNY-site during July 28-30, 2019. At Stony Brook in the NLI, air temperatures at noon and in the afternoon are clearly lower than those at CCNY. As shown by the windroses maps in Fig.3(c-d) at CCNY-site, the wind directions were prevailing northwest on July 25-26 but southwest in the daytime on July 28-30; this indicates that the SLI area was located in the NYC downwind area on July 25-26 whereas the NLI coast and Long Island Sound were located in the NYC downwind area on July 28-30. Therefore, the O_3 concentrations at the NLI and SLI area are affected differently by the NYC urban emissions and pollutants transport. In addition, at

Stony Brook weather station in the NLI, the prevailing Northwestern and North winds were shown before 3:00 pm EDT on July 28-29 (**Fig.S2 in Supporting Document**), which indicates the on-shore winds from Long Island Sound or the sea-breezes to the coastal area. Thus, the high O_3 on July 28-30 at the NLI (Eatons Neck, Flax Pond and Riverhead shown in Fig.S2 (e)) are associated with the combined effects from the urban pollutants transport and sound-breezes that may form a convergence zone along the coast for the O_3 accumulation.

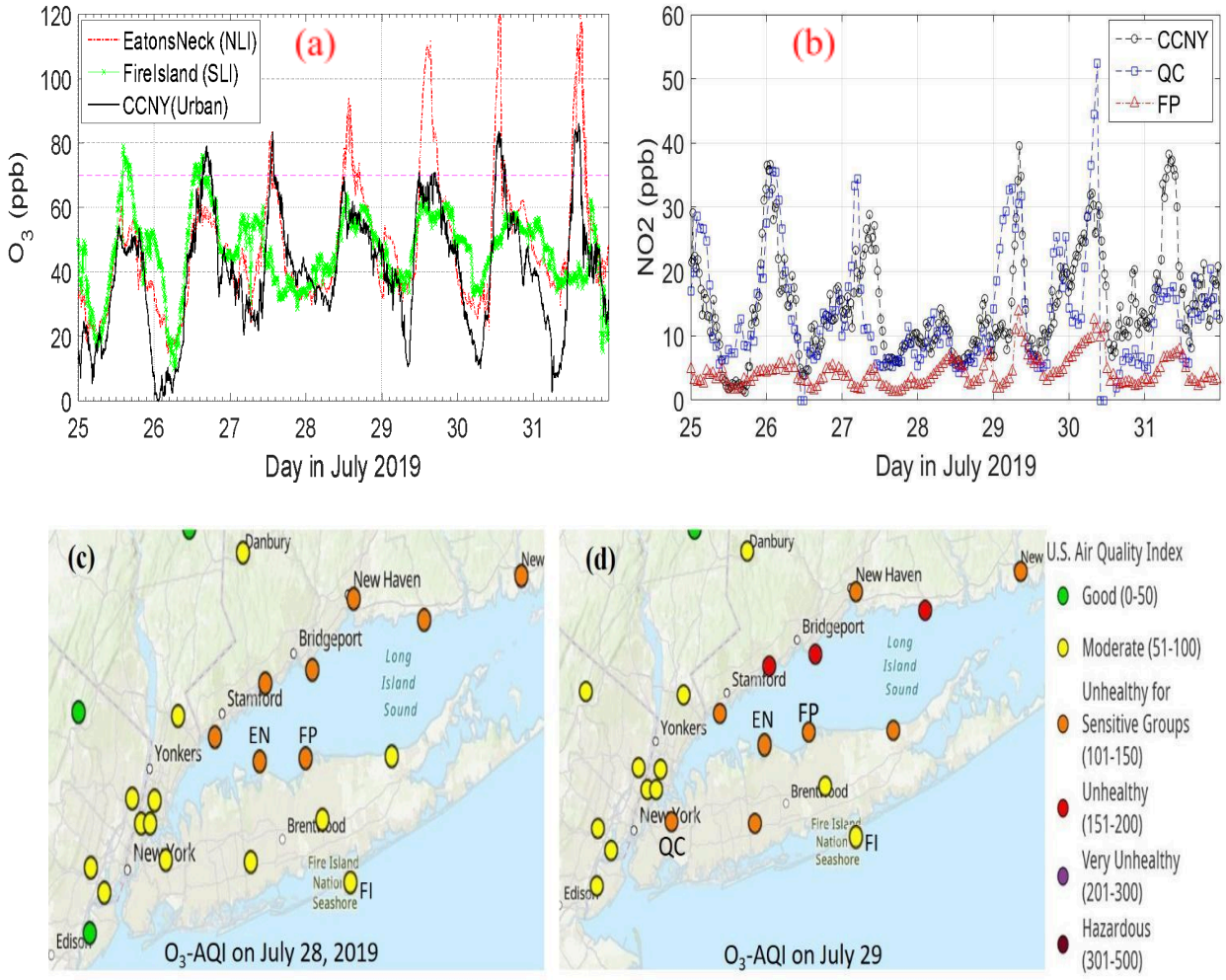

Fig. 2. Temporal variation of (a) near-surface O_3 and (b) NO_2 in the NYC urban and coastal area in Long Island during July 25-31, 2019; (c)-(d) Daily O_3-AQI on July 28 and 29, 2019 from AirNow. FP-Flax Pond, QC-Queens College, EN-Eatons Neck, FI: Fire Island (see Fig.1 and Table-1 for the site full names and locations.)

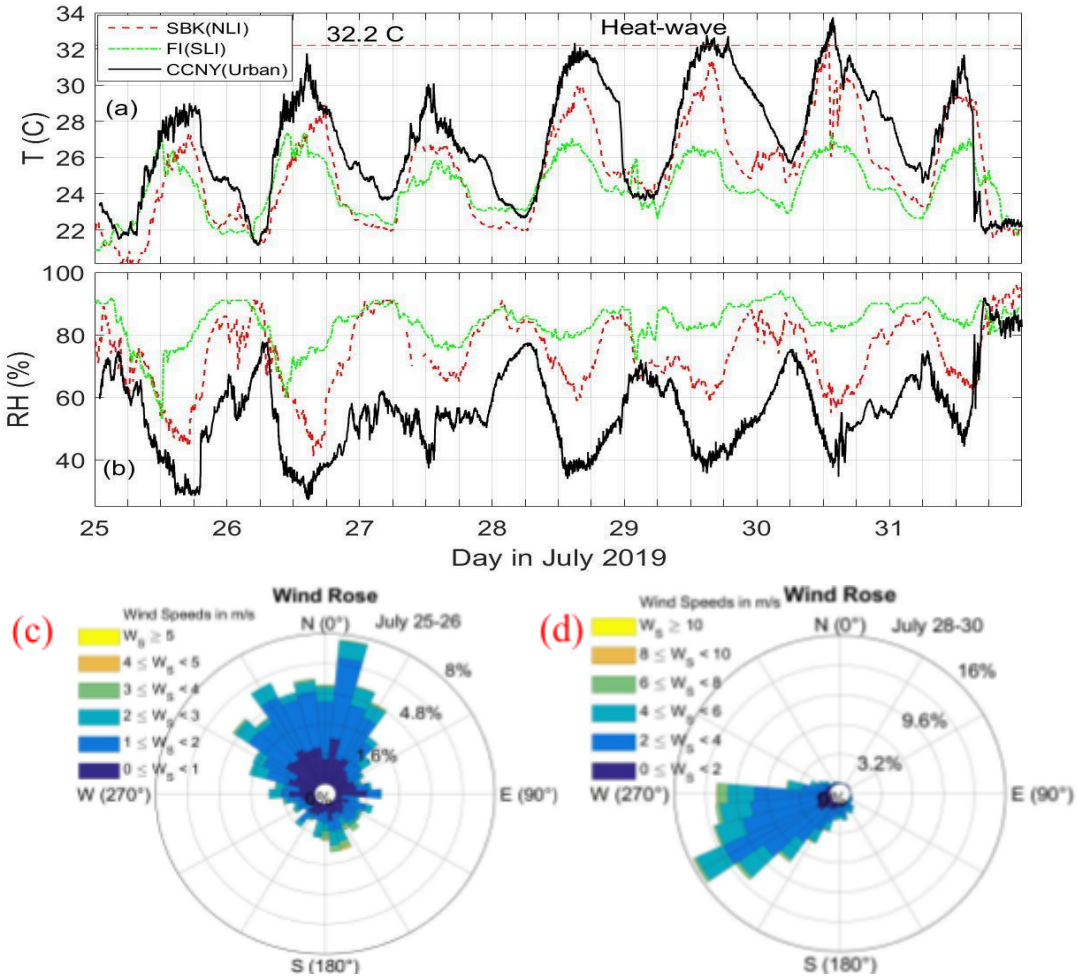

Fig. 3. (a)-(b) Air temperature and RH at CCNY (1-min ave.), Stony Brook (SBK in NLI) and Fire Island (FI in SLI), (c) Wind rose at 6:00-18:00 EDT on July 25-26 and (d) July 28-30 at CCNY (Urban).

3.2 PBLH estimate and diurnal variation in the NYC urban and coastal area

Figure 4 shows the inter-comparison of MLH or PBLH measured from the ceilometer, wind lidar and virtual potential temperature (VPT or θ_v) and water vapor (H_2O) profiles of the radiosonde/ozonesonde at the NLI on July 29, 2019. The ozonesonde measured VPT and H_2O profiles at around 14:30 UTC (10:30 local time or eastern daylight time-EDT) and 19:15 UTC (15:15 local time), and the PBLH is estimated from the sharp increase of VPT and the large decrease of H_2O mixing ratio. In the morning, the PBLH are consistently low from these methods. For the convective boundary-layer (CBL) at 19:15-19:20 UTC, the estimated MLH was 2.0 km from the ceilometer, 1.75 km from the wind lidar and 1.91 km from VPT profile, respectively. Some limitations on the MLH estimate from ceilometer and wind-lidar data can be seen. For instance, for the ceilometer data or method (Fig.4a), following the rains or shower around 4:00 UTC, some aloft aerosol plumes at 6:00-12:00 UTC can be seen while at about 16:00 UTC there are low clouds at around PBL-top; both aloft aerosol plumes and low-clouds induce noise on the MLH estimate. On the other hand, the lower MLH from the wind lidar might be due to lower aerosol loading at the PBL-top (Fig.4b-top, signal intensity or CNR). During the CBL period, the MLH estimates from the wind lidar are not sensitive to the selected threshold values. However, for the stable boundary layer (SBL), the vertical velocity variance method used in the wind lidar becomes incapable due to weak vertical mixing or turbulence (Fig.4b-middle); in this case the method using the vertical gradient of horizontal wind

speeds can give the SBL height as shown in Fig.4b-bottom. For the CBL period on this day, the PBLHs from the horizontal wind gradient method show good consistency with those from the vertical velocity variance method (Correlation coefficient R=0.85). Another case study for the PBLH comparisons on July 28 is given in **Fig.S3 in Supporting Document**, which shows similar comparing results in Fig.4. Table-2 lists the comparisons in detail on July 28-29, 2019. Overall, the methods from the ceilometer, wind lidar and potential temperature profile show good consistency of MLH for the convective PBL at noon and afternoon. However, in the early morning or later afternoon, the PBLHs become lower for the stable boundary layer, the different methods indicate large relative bias. On the other hand, their bias might be partially attributed to different range resolutions, lowest detecting altitudes and observation locations.

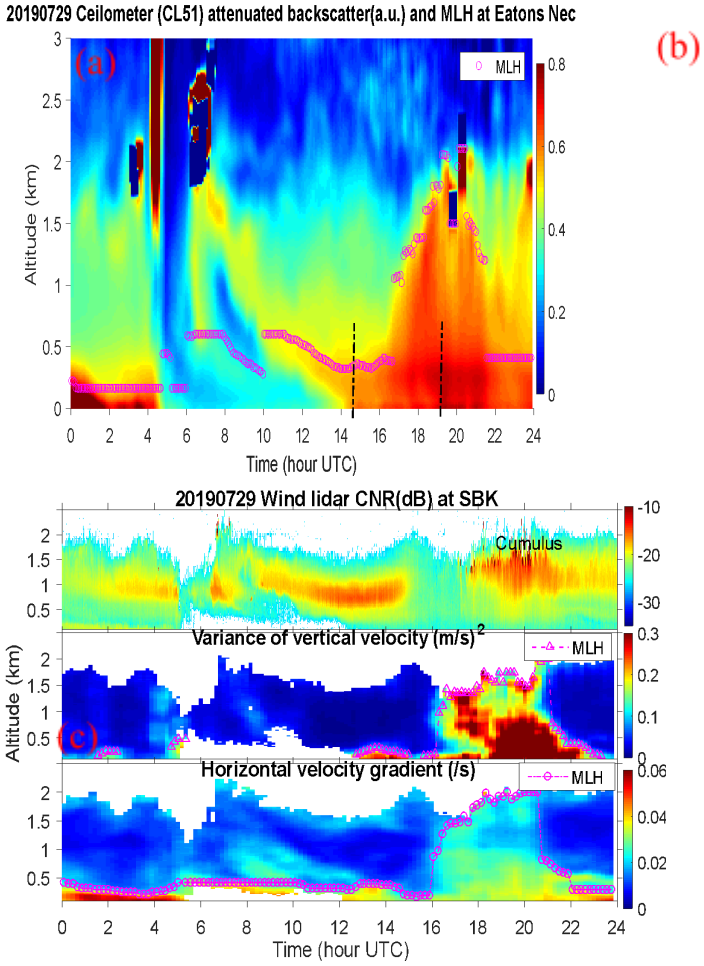

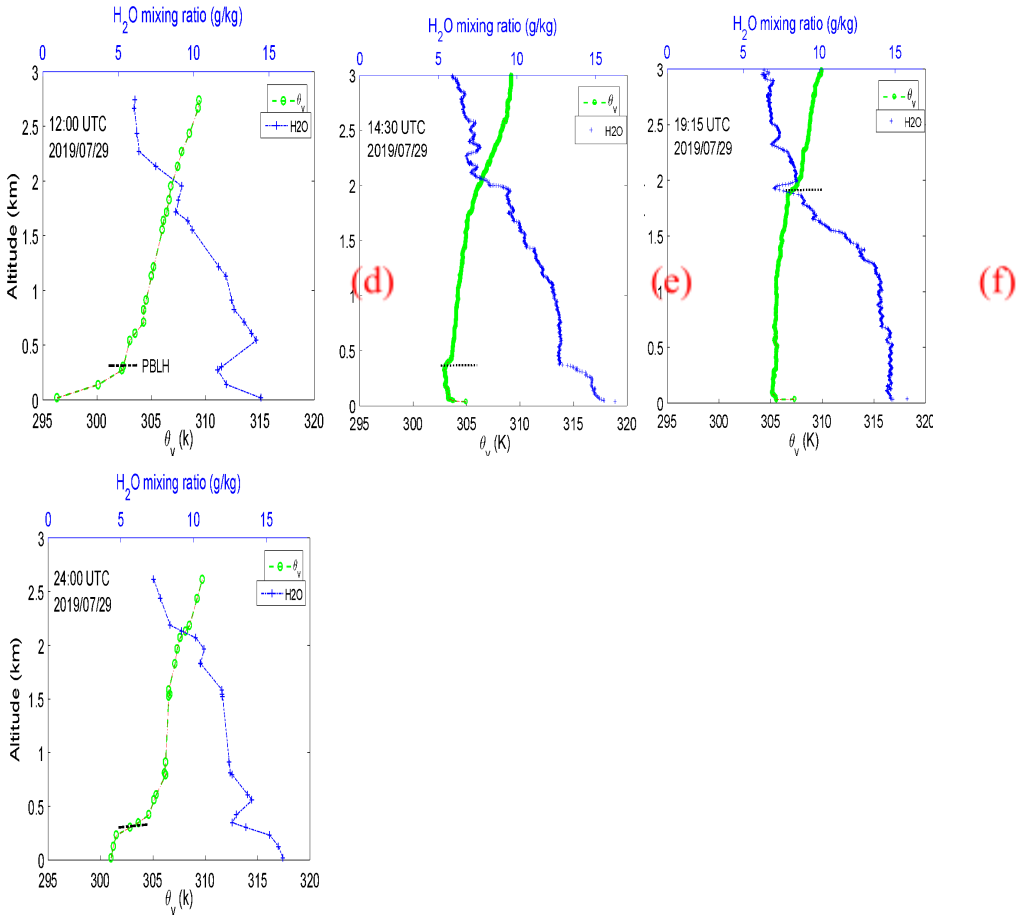

Fig.4. Comparison of MLH measured from the methods of (a) Ceilometer, (b) Wind lidar, (c–f) Virtual potential temperature (θ_v) and water vapor (H_2O) profiles at the North-shore of Long Island on July 29, 2019. (Vertical dash lines in Fig.4 (a): ozonesonde launch time; horizontal dash lines in (c-f): PBLH)

Figure 5 gives the vertical distribution profiles of aerosol total scattering coefficient at 550 nm, virtual potential temperature (Θ_v), and water vapor (H_2O) measured from the UMD research aircraft near Flax Pond on July 29 (time 19:32-19:52 UTC). The PBLH is calculated with the value of 1.7 km from aerosol profile, 1.63 km from the Θ_v method, and 1.85 km from the vertical gradient of H_2O. They generally agree well with the relative difference from the aerosol profile method less than 10%.

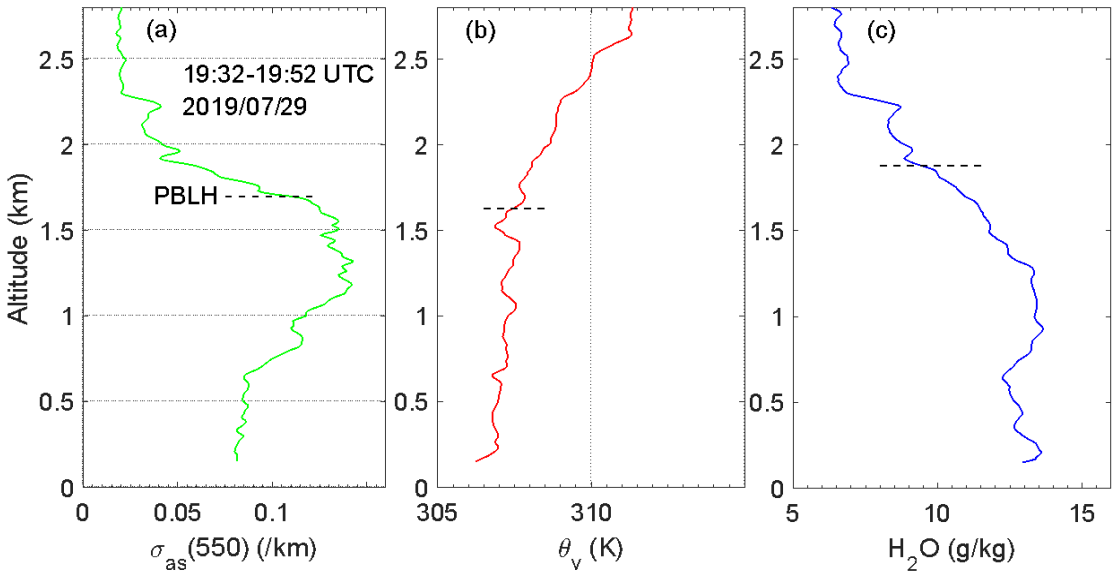

Fig.5. Vertical profiles of (a) aerosol total scattering coefficient (σ_{as}) at λ=550-nm, (b) virtual potential temperature (θ_v), and (c) water vapor (H_2O) measured from the UMD research aircraft near Flax Pond at 19:32-19:52 UTC on July 29, 2019. (Horizontal dash lines – PBLH estimate from each method)

Table-2. PBLH comparison among the methods from ceilometer, wind lidar and virtual potential temperature (θ_v) at the North-shore of Long Island (UTC-4=local time or EDT)

	July 28 (UTC time, hour : min)			July 29 (UTC time, hour : min)			
PBLH (km)	12:00 (SBL)	20:00 (CBL)	24:00 (SBL)	12:00 (SBL)	14:30 (CBL)	19:20 (CBL)	24:00 (SBL)
PBLHθ_v	0.38	1.94	0.37	0.30	0.38	1.91	0.33
$PBLH_{CL}$	0.36	2.01	0.35	0.52	0.335	2.05	0.41
$PBLH_{WL}$	0.30	1.80	0.40	0.20	0.30	1.75	0.20

Subscripts Θ_v: Virtual potential temperature method; CL: Ceilometer method; WL: Wind lidar method. The PBLH is equivalent to MLH for the Convective Boundary Layer (CBLH) (Stull, 1988).

Figure 6 gives the ceilometer-measured attenuated backscatter intensity and MLH and at CCNY, Eatons Neck and Fire Island during July 26-31, 2019, respectively. These backscatter intensities are relative values since they are not yet calibrated with the instrument constant. It can be seen that the MLHs increase from 0.3 to 2.0 km at 10:00 am to 2:00 pm EDT on July 28 and 29 at CCNY; and the maximum MLH is much higher at CCNY (~2.0 km) than at Eatons Neck (~1.65 km) on NLI and Fire Island on SLI. The MLH is at the lowest level at Fire Island along with residual aerosol layers (aerosol layer height - ALH in Fig.6c), which corresponds to much lower air temperature (Fig.3a). In addition, at these three-site, the aloft aerosols plumes and low-clouds can be seen on July 27-31, and some rain or showers occurred in the early morning of July 29, noon on July 30 and 31. Unfortunately, there are no data records at Eatons Neck from the night of July 29 to noon of July 30 due to the data transfer issue from the instrument to computer. Below we focus on the comparison analysis of MLH and O_3 in the NYC urban and North-shore of Long Island (NLI) on July 28-30, 2019 since the ground O_3 are at the highest levels in the NLI and there are the O_3 and meteorological profile data available from the ozonesonde and UMD research aircraft in the NLI.

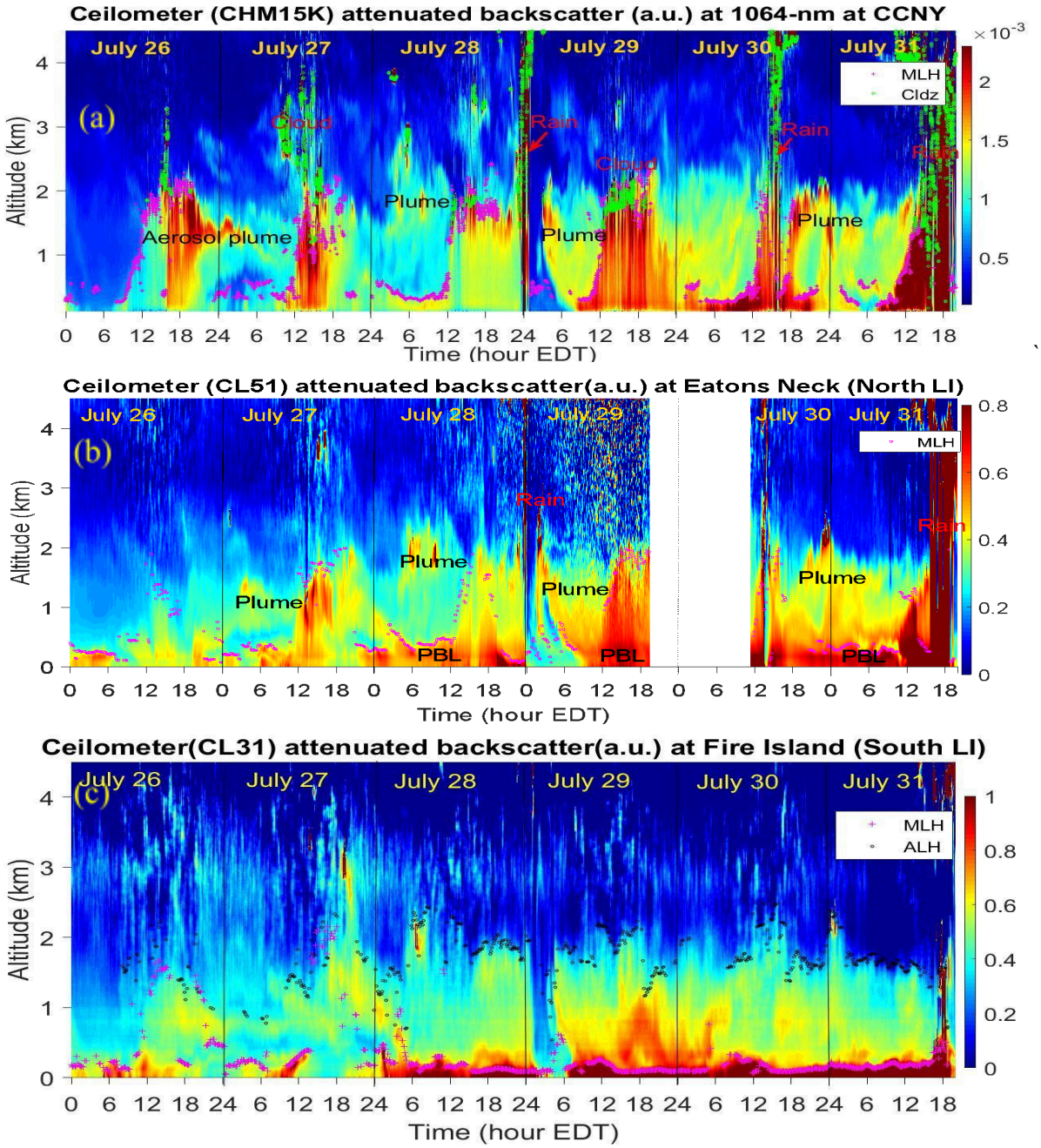

Fig. 6. Ceilometer-measured backscatter intensity (relative values) and MLH at (a) CCNY, (b) Eatons Neck, and (c) Fire Island during July 26-31, 2019. (MLH: mixing-layer-height; Cldz: cloud base; ALH: aerosol-layer-height)

We made the comparison and correlation analysis of the MLH between the ceilometer and wind lidar methods at the NYC urban and NLI coastal area on July 28-30, 2019, respectively. **Figure 7** shows their temporal variations and the linear regression. At both two areas, the MLHs from the ceilometer and wind lidar show consistent diurnal variation. In the NYC urban area as shown in Fig.7b, the MLHs from the ceilometer and wind lidar show strong linear correlation with the regression slope of 0.99 and correlation coefficient of R=0.9. In the coastal area in NLI as shown in Fig.7d, the MLHs in the convective PBL period are slightly underestimated from the wind lidar in comparison to the ceilometer, their linear

correlation coefficient is 0.81 and the linear regression slope is 0.67. In the coastal area, the vertical convection intensity is relatively weak and the aerosol loadings are less than those in the urban area, thus the estimated MLHs from the wind lidar and ceilometer show a moderate correlation and reasonable consistency.

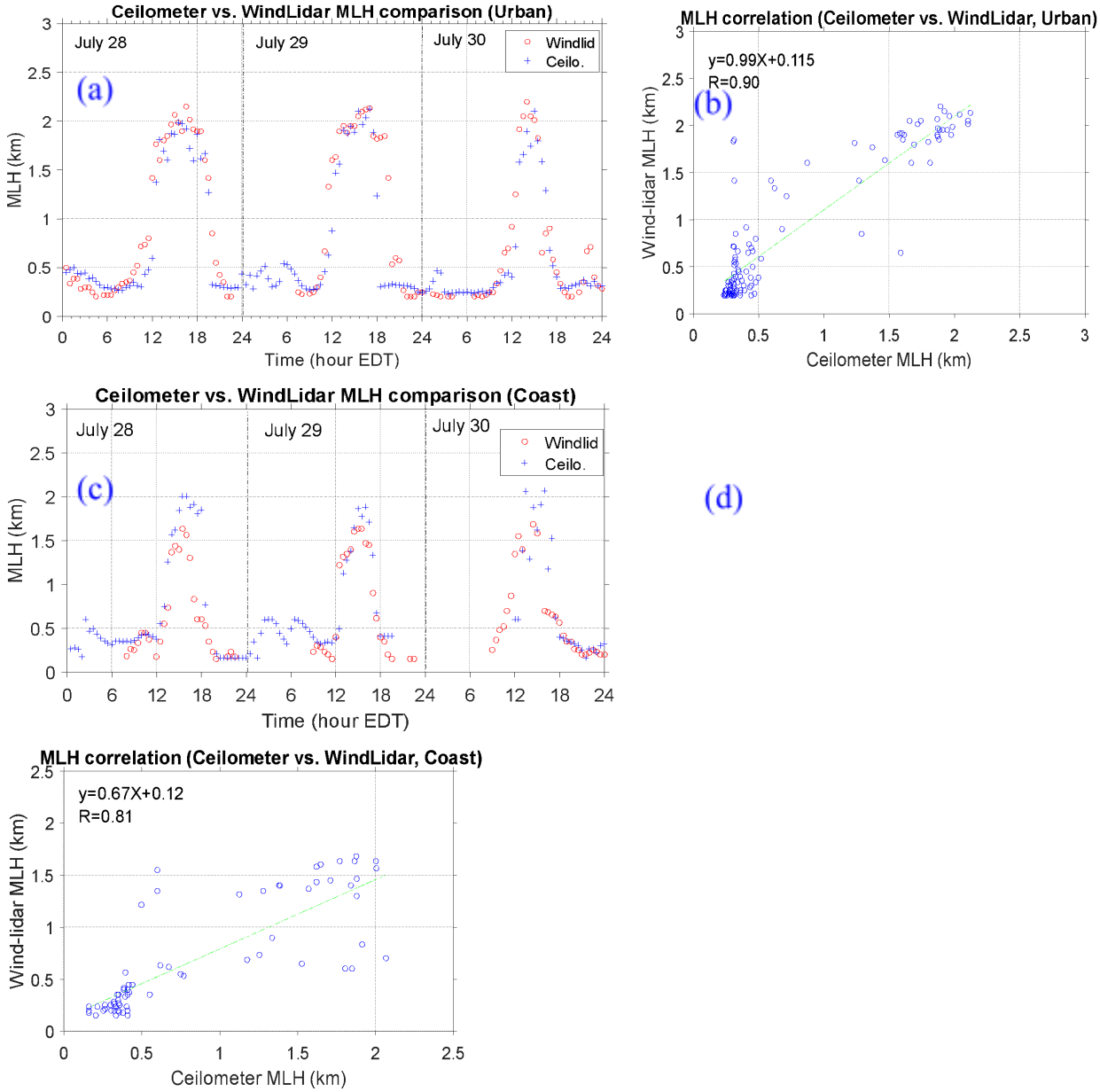

Fig. 7. Comparison and correlation of MLH (30-min ave.) between the ceilometer and wind-lidar methods in the NYC urban (a-b), and the NLI coastal area (c-d), respectively.

Figure 8 shows the diurnal variation and comparison of ground-level O_3 and MLH in the NYC urban and coastal area in NLI on July 28-30, 2019. In comparison to the NYC urban area, the maximum O_3 concentrations are much higher in the coastal area (Fig.8a) whereas the MLHs are much lower at noon and in the afternoon (Fig.8b). Meanwhile, the MLHs start to grow earlier from the mid-morning to noon in the urban area than the coastal area (Fig.8b). High MLH in the urban area is generally due to hot surface and strong vertical mixing. As shown in Fig.8c, the ratios of vertical velocity variances at the

urban to those in the coastal area indicate much stronger vertical convection during the PBL transition periods (10:00-13:00 and 17:00-19:00 EDT) in the urban area. As for July 29, the MLH grows from 0.25 to 2.0 km altitude at 10:00-11:30 EDT in the urban area, but rises from 0.2 to 1.7 km from 12:00 to 15:00 EDT in the coastal area. At noon and early afternoon (convective PBL), the average MLH is at 2.0±0.1 km at 13:00-17:00 EDT in the urban area, but becomes lower with the average of 1.5 ± 0.14 km at 13:00-16:00 EDT in the coastal area. During the time period above, the ground O_3 concentrations keep increasing in the coastal area but become stable in the urban area (Fig.8a). Lower MLHs in the coastal area indicate smaller air volumes for the O_3 dilution or dispersion thereby partially resulting in higher O_3 at near-surface.

We calculated the integrated O_3 content (IOC) in the PBL at noon time when both PBL height (PBLH) and surface O_3 attain the maximum values. The O_3 might be assumed to be well mixed due to strong turbulence mixing in the PBL. Subsequently, the integrated O_3 content (IOC) in the PBL at noon can be calculated with the PBLH or MLH multiplying surface O_3 concentration. The comparison of IOC may indicate the PBL-height impact on the surface O_3 at noon since the PBLH generally defines the air volume for surface O_3 dilution. However, the uncertainty of such comparison depends on the O_3 vertical distribution and local chemical process for O_3 production. On July 28 (14:00-16:00 EDT), the average IOC is 114.8 ± 6.3 ppb×km at CCNY-site (urban) and 112.4 ± 11.2 ppb×km at Eaton Neck (coast), respectively. On July 29 (13:00-16:00 EDT), the average IOC is 127 ± 9.9 ppb×km at CCNY and 159 ± 20 ppb×km at Eaton Neck. Therefore, they generally show good consistency at noon time in the urban and coastal area.

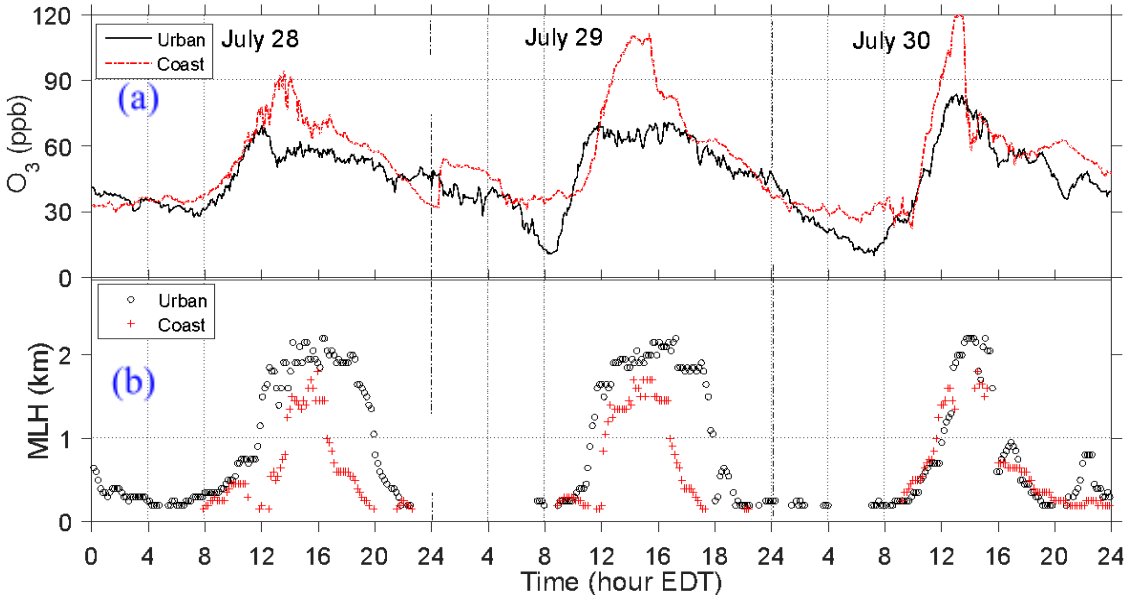

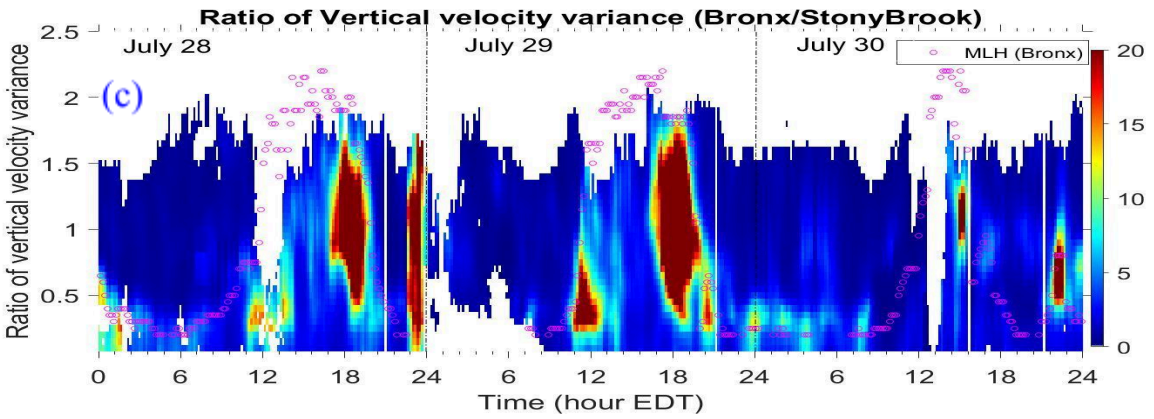

Fig. 8. Diurnal variation of ground O_3 (a), MLH (b), and (c) Ratio of vertical velocity variance from the wind lidar measurements in the NYC urban and the coastal area in North-shore of Long Island (NLH) on July 28-30, 2019 (red circles: MLH in the urban area).

3.3 Horizontal winds and vertical mixing in the PBL

Figure 9 and 10 show the wind-lidar measured backscattering intensity or carrier-noise-ratio (CNR), horizontal wind speed, direction, and vertical velocity in the NYC urban and the coastal area in NLI during July 28-31, 2019, respectively. Fig.9 (a) indicates the lidar detection altitude, cloud and rain information (stronger backscatter). First, the horizontal wind directions indicate the prevailing southwest (SW) in the NYC urban area (Fig.9c) but the northwest (NW) before 15:00 EDT in the lower PBL at Stony Brook (Fig.10c) on July 28 and 29. This means that the NLI area suffers from the downwind transport of NYC urban plumes; meanwhile, the prevailing Northwest winds below 0.4 km altitude at 10:30-15:00 EDT on July 28-29 in Fig.10(c) indicate the sea breezes from Long Island Sound that prevent the off-shore dispersion of the pollutants. In addition, the surface weather observations at the Stony Brook campus also indicate that the prevailing NW winds occur before 15:00 EDT on July 28 and 29, 2019 (**Fig.S2 in Supporting Document**). Furthermore, the vertical velocity variances indicate much weaker vertical mixing in the NLI than those in the NYC urban area (not shown here), particularly in the time period of MLH morning transition. Therefore, the urban pollutants transport, low MLH, weak vertical mixing and sea-breezes provide the beneficial meteorological conditions for the O_3 accumulation in the North-shore of Long Island. The chemical production and deposition process of O_3 may also affect spatial patterns of O_3 in the coastal area, which is out of the scope of this paper.

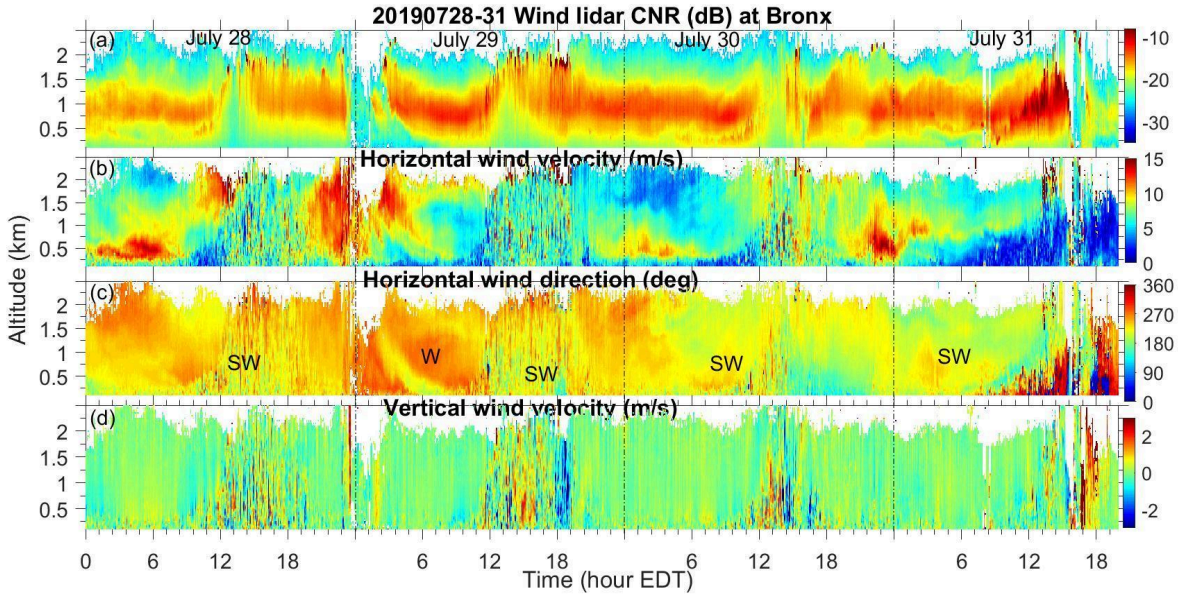

Fig.9. (a) Wind lidar measured carrier-noise-ratio (CNR), (b) horizontal wind speed, (c) wind direction, (d) vertical wind velocity (+up, –down) at Bronx (NYC urban site) during July 28-31, 2019.

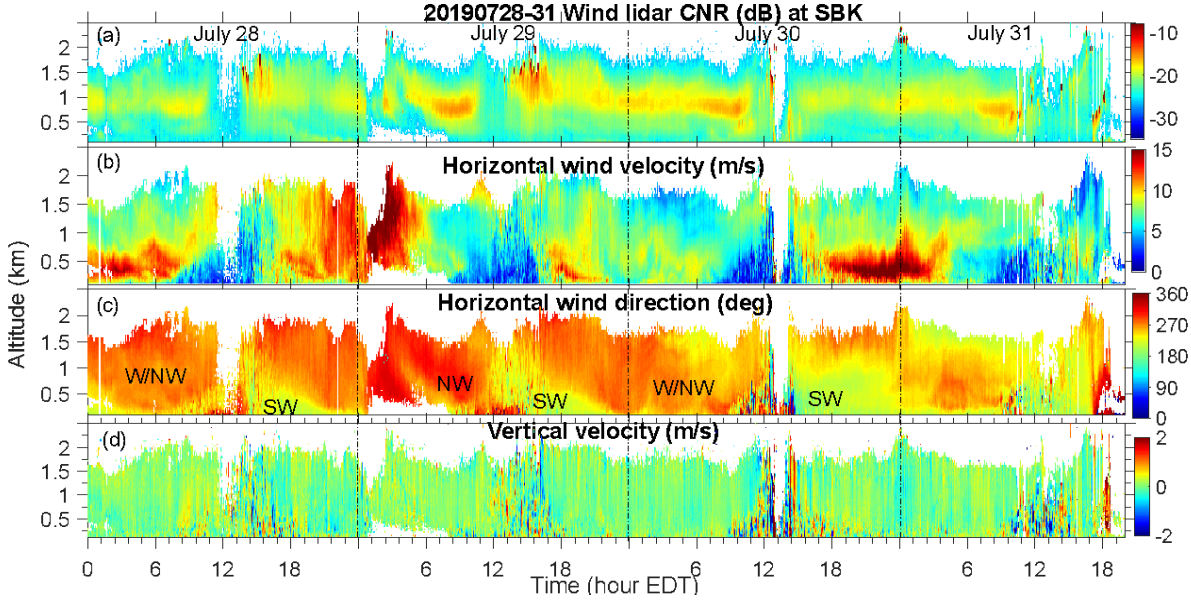

Fig.10. Same as Fig.9 except at Stony Brook (SBK) in the Northern Long Island (NLI). (The prevailing Northwest winds below 0.4 km altitude at 10:30-15:00 EDT on July 28-29 in Fig.10(c) indicate the sea breezes from Long Island Sound, please refer to the site location in Fig.1.)

3.4 Vertical profiles of O_3 and other gaseous compounds

Figures 11 and 12 show the vertical distribution of O_3 and winds measured from the ozonesondes at Flax Pond on July 29, 2019 (14:29-14:40 UTC in the morning and 19:14-19:22 UTC in the afternoon), respectively. The corresponding virtual potential temperature and H_2O profiles are referred in Fig.4 (d)-(e). The O_3 mixing ratio profile shows slight variation below 3-km altitude in the mid-morning with the concentration of 60-62 ppb (Fig.11a); prevailing winds are out of the NW near the surface (Fig. 11b). However, a significant increase of the O_3 can be seen with the mixing ratios of 83-102 ppb in the

afternoon (Fig.12a). Moreover, Fig.12a indicates higher O_3 in the upper PBL than at near-surface (<0.5 km), which might be associated with the dramatic variation of horizontal wind direction and speed (prevailing SSW and weak winds below 0.5 km but WSW stronger speed above 0.5 km).

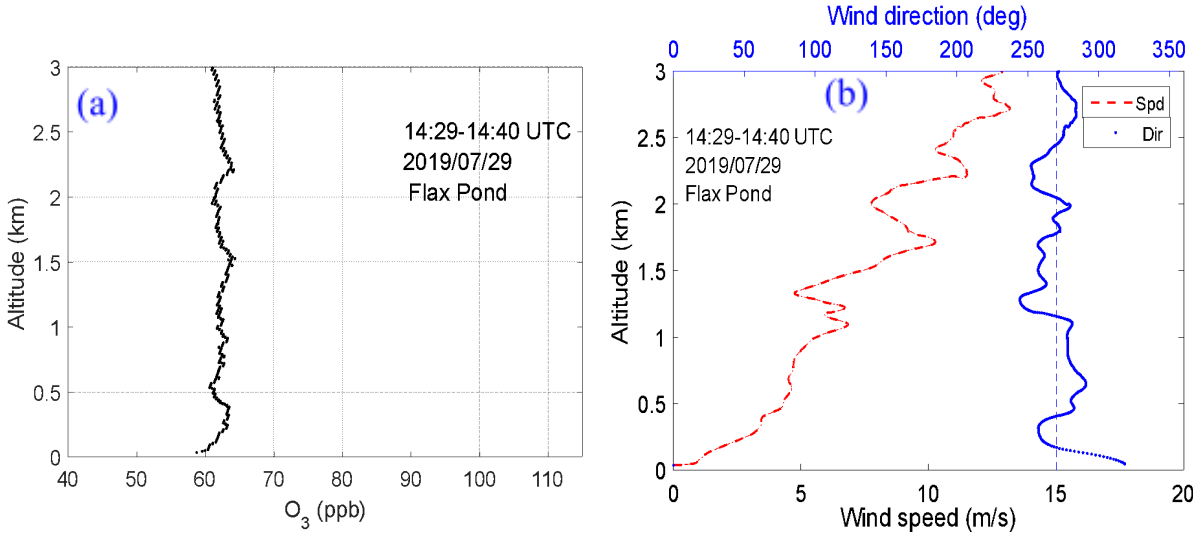

Fig.11. (a) Vertical distribution of O_3, (b) wind speed (Spd) and direction (Dir.) measured from the ozonesonde at 14:29-14:40 UTC on July 29, 2019 (vertical dash: wind direction at 270º).

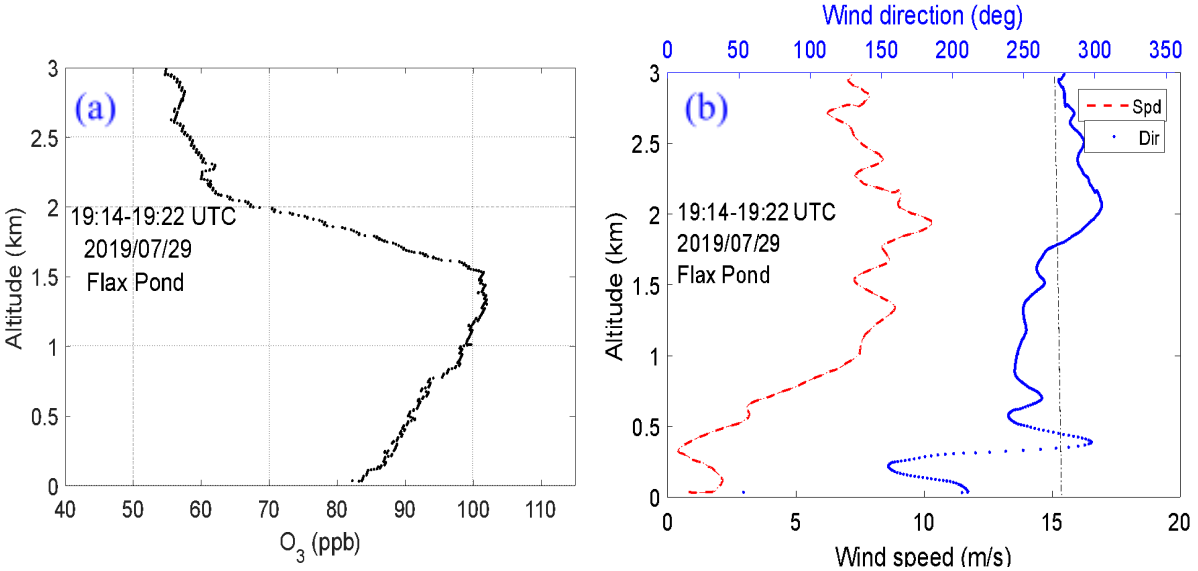

Fig. 12. (a)-(b) Same as Fig.11 except at 19:14-19:22 UTC on July 29, 2019 (afternoon).

Figure 13 shows the vertical distribution of O_3, CO, NOx, HCHO, and aerosol scattering coefficient measured by the UMD research aircraft in the afternoon of July 29, 2019; and the corresponding flight track and time-height are given in Fig. 13(a). The flight time for the two vertical profiles (aircraft spiral up and down) is at 19:32-20:15 UTC; the ascent (green track in Fig. 13a and P1 in Fig. 13 (b-g)) is located nearby Flax Pond on the North-shore of Long Island while the descent (red track in Fig. 13a and P2 in Fig. 13 (b-g)) starts from the North-shore of Long Island, then crosses Long Island Sound and finally lands inland on Long Island. As shown in Fig. 13 (b), the O_3 mixing ratios are much higher with the value of 110-120 ppb in the PBL in the North-shore of Long Island (P1-green) than other area

(P2-red). Concentrations of CO, NOx, HCHO, CH_4, and aerosols are also higher over the North-shore of Long Island (Fig.13(c-g)). Ozone shows slight variability in the PBL whereas the aerosols and other gaseous compounds show a little larger values at 0.6 km-1.5 km altitude than those below 0.5 km altitude. The larger aerosol backscatters could be related to the local RH maximum. Profiles of black carbon (BC), virtual potential temperature, and water vapor are given in **Fig. S4 in the Supporting Document**, these indicate more BC over NLI. These coincident high-levels of O_3, CO, NO_x and HCHO in the PBL indicate the transported urban plumes; and the high-level O_3 agrees well with the ground measurements at Eatons Neck and Flax Pond in NLI area but differ from the ozonesonde measured O_3 profile near the surface (inland of LI) (**Fig.12**). The spatial homogeneity of O_3, CO, NO_2 and BC is illustrated from the low-level flight measurements (e.g., flight altitude **at 0.15-0.36 km at 18:32-20:22 UTC** in the afternoon on July 29), and the results indicate higher concentrations of O_3, CO and BC near the Shoreline along Eatons Neck and Flax Pond (**See Fig.S5 in Supporting Document**); the CO and BC concentrations are even higher in the North-shoreline of LI than those near NYC urban area. In addition, the transported wildfire smoke plumes are indicated from the lidar-ceilometer and NOAA fire and smoke product (**See Fig.15 below and Fig.S6 in Supporting Document**) in NYC urban and Long Island Sound area, which may indicate the urban plumes mixing with the transported smoke in the NYC and Long Island Sound area.

3.5 Spatial distribution of NO_2, HCHO and aerosols from satellite sensors

Figure 14 gives the spatial distribution of tropospheric column contents of NO_2 and HCHO measured from satellite S5P/TROPOMI on July 28 and 30, 2019 (no retrievals available on July 29). The results indicate higher NO_2 and HCHO in the NYC urban area and North-shore of Long Island on both days, which is qualitatively consistent with higher NOx and HCHO concentrations in the PBL observed by the UMD aircraft around Flax Pond. In addition, the satellite MODIS/Aqua RGB images show clear sky over Long Island Sound but a line of clouds in Long Island (**Fig.S7 in Supporting Document**), which generally indicates the sea-breeze front (Bao et al., 2023). Therefore, higher NO_2, HCHO, CO and aerosols from the aircraft and satellite data likely indicate a convergence zone in the North-shore of Long Island where the transported O_3 and other urban pollutants could be accumulated.

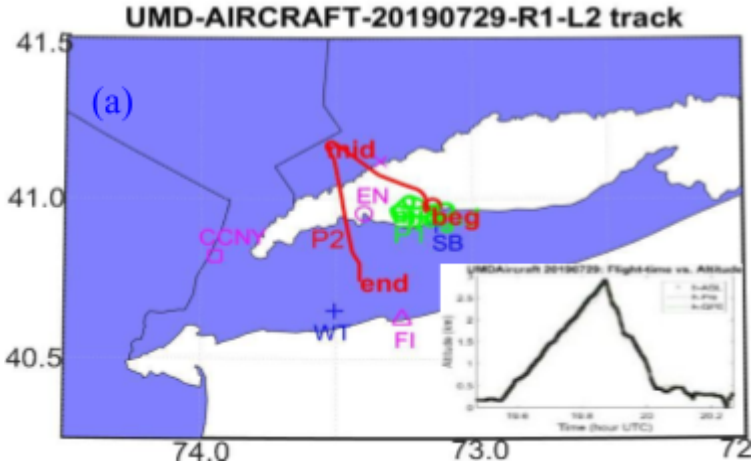

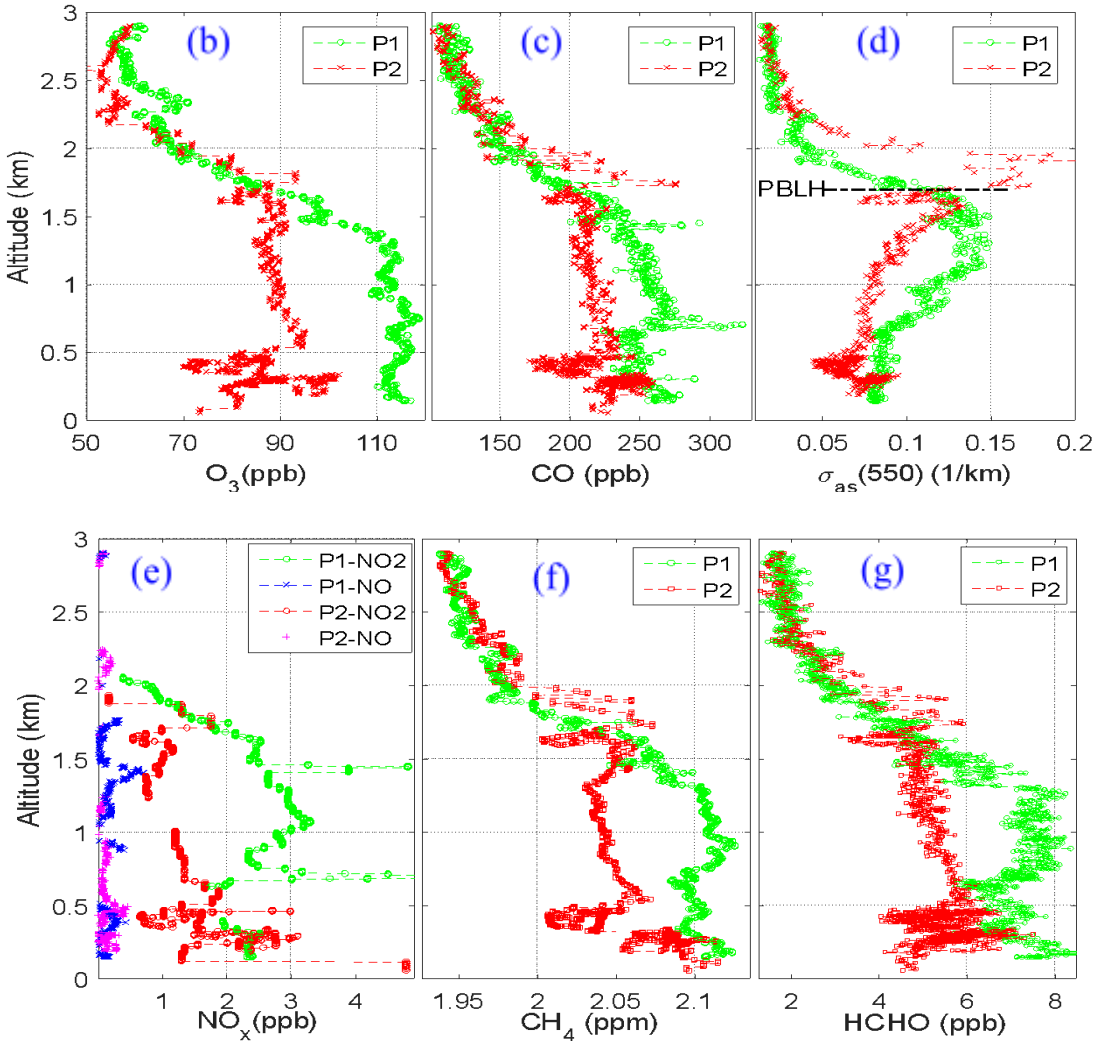

Fig.13. (a) Aircraft flight track and time-height for the two vertical profile measurements (P1- ascent in green; P2- descent in red), (b)-(g) Profiles of O_3, CO, aerosol scattering coefficient (σ_{as}, horizontal dash-PBLH), NO_x, CH_4, HCHO on July 29, 2019. P1: ascent at 19:32-19:52UTC near Flax Pond; P2: descent at 19:52-20:15UTC cross LIS.

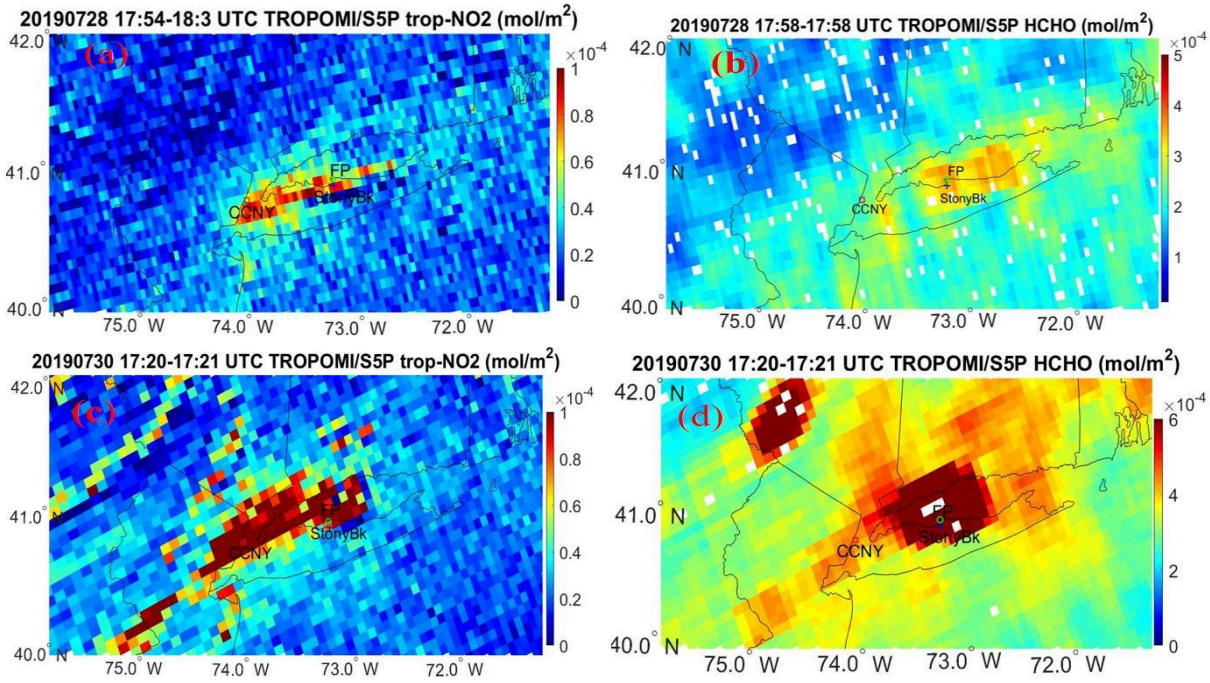

Fig.14. (a)-(d). Tropospheric column content of NO_2 and HCHO measured from S5P/TROPOMI/ on July 28 (a, b) and 30, 2019 (c, d).

In addition, the transported wildfire smoke plumes were indicated by CALIPSO and NOAA-HMS Fire and Smoke product as shown in Fig.S8 in the Supporting Document. **Fig.S8** (a)-(b) shows the range-resolved total attenuated backscatter and aerosol types measured from the satellite CALIPSO in the east coastal area around NYC in the early morning of July 30 (2:00 am local time) or in the late night of July 29, 2019. The results indicate some aloft smoke plumes in the PBL that are classified by aerosol optical properties around the NYC and LIS area. Furthermore, the NOAA Hazard Mapping System (HMS) fire and smoke product indicates the smoke intrusion (light-moderately dense) to the NYC area (Fig.S8c), the lighter density (usually far downwind) HMS smoke polygons are decoupled from the surface (Liu et al, 2023).. In addition, the NOAA-HYSPLIT ensemble backward trajectories show that the air at 2-km altitude at CCNY mostly originated from the Northwest US and Canada and traveled for 7-days. On the other hand, the NOAA HRRR-smoke model forecast shows light-moderate levels of smoke intrusion to the NYC/LIS region during July 26-29, 2019 (the images available at https://rapidrefresh.noaa.gov/hrrr/HRRRsmoke/). In addition, the wildfires and smoke plume were observed on July 22-25, 2019 in the Northwest US during the FIREX-AQ campaign (Crawford, et al., 2021; June et al., 2022). Overall, these satellite observations and the model predicted results demonstrate high levels of NO_2, HCHO and aerosols in the North-shore of Long Island, and indicate the transport of the NYC urban plumes and the aged wildfire smoke plumes.

3.6 **Evaluation of WRF-Chem and NOAA NAM-CMAQ modeling O_3 and PBLH**

At last, we made the comparisons of ground O_3 and PBLH between the WRF-Chem model (1.3 km grid), NOAA NAM-CMAQ (12 km grid) model forecast and the observations at the coastal area in Long Island (Riverhead and Babylon sites) and NYC urban area (CCNY-site) during July 28-30, 2019. **Fig.15** shows the comparisons of O_3 at Riverhead and Babylon sites. It can be seen that there is a time-lag of 2-3 hours for the maximum O_3 timing from the NAM-CMAQ model, but the WRF-Chem products show good consistency with the observations. In addition, at the coastal site as shown in Fig.15c, the PBLH from the

NAM-CMAQ model are generally lower than the observation data at noon and in the afternoon. During the morning transition period or PBLH growing period, the PBLHs from the NAM-CMAQ model product start to grow earlier than the observation data, which might partially affect the predicted O_3 concentrations near the surface. On the other hand, in the urban area (CCNY-site), the NAM-CMAQ modeled O_3 values show consistent timing for the maximum O_3 with the observation (See **Fig.S9 in the Supporting Document**). However, the night-time O_3 from the WRF-Chem predictions are over-estimated. In addition, the comparisons of the air temperature and wind between the models and observations at CCNY are shown in **Fig.S10 in the Supporting Document;** and the results indicate that the modeling temperature and horizontal wind direction agree well with the observation whereas the horizontal wind speeds are over-predicted by the model. Torres-Vazquez (2022) evaluated the WRF-CMAQ simulation performance of the meteorology and O_3 for LISTOS 2018, and the two cases studies suggest that higher spatial resolution (1.3 km grid) improved surface meteorology simulation throughout the whole summer. Further sensitivity and comparison analysis of the model simulations are highly recommended with different spatial resolutions, emissions and meteorological initiation at the coastal area, this is out of this study and will be explored in a separate research.

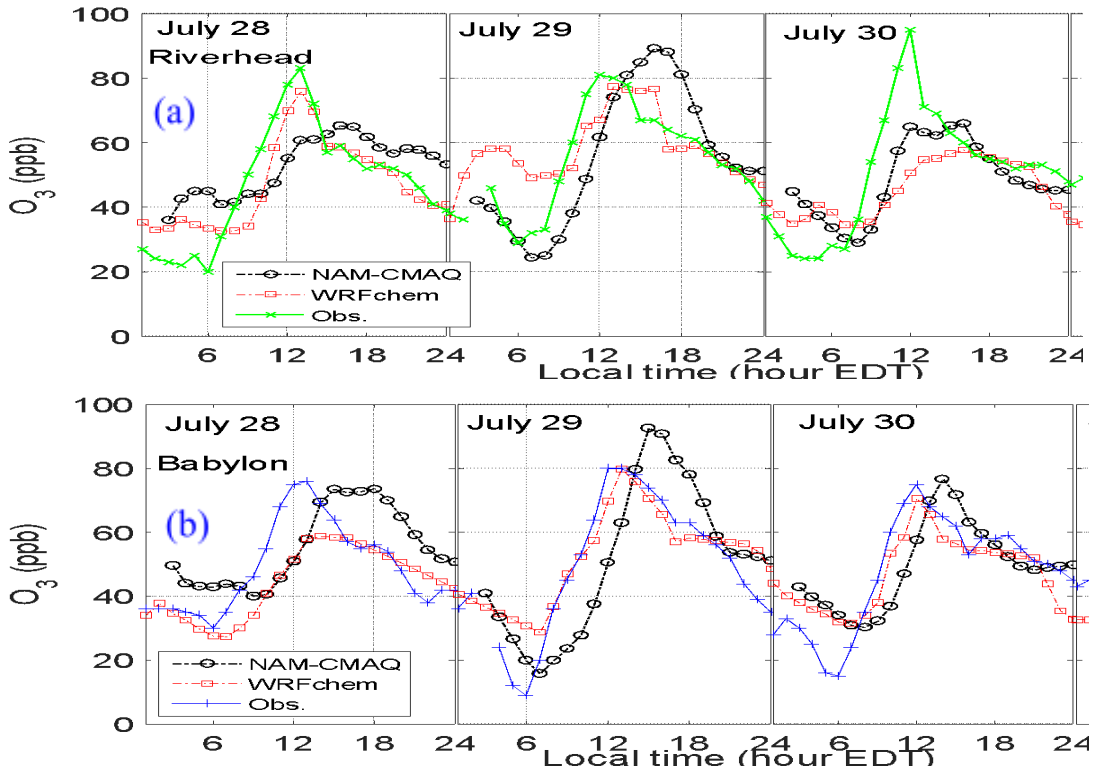

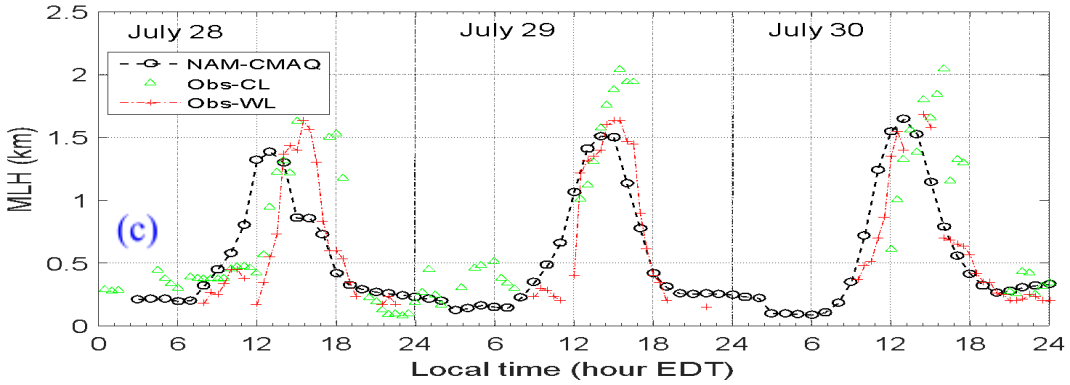

Fig.15 (a)-(b) Comparisons of ground-level hourly O_3 between the WRF-Chem, NAM-CMAQ model and the observations, (c) MLH comparison in the coastal area of Long Island during July 28-30, 2019.

4. Conclusions

This study presents the integrated observations and comparisons of O_3 and PBLH diurnal variation in New York City and its downwind coastal area in Long Island Sound. The multi-platform measurements are used to investigate the PBL dynamics for a persistent O_3 episode during July 28-31, 2019, which includes the research aircraft, wind lidar, ceilometer, aerosol lidar, ozonesonde and in-situ samplers. The results indicate that higher O_3 in the North-shore of Long Island (NLI) is associated with lower PBLH, urban pollutant transport and land-sea breezes.

For the convective boundary layer, the methods from the ceilometer, wind lidar and potential temperature profile obtain consistent PBLH or MLH by showing their absolute differences at around 100-200 m and strong correlation (R>0.8). However, for the stable boundary layer in the morning and night in the NLI, it becomes a challenge to estimate the low PBLH using the variance of vertical velocity whereas the method with the vertical gradient of horizontal wind speed can obtain a reasonable result. The ceilometer can report a reasonable PBLH except for some contamination or noises from aloft aerosols and low clouds. In addition, the PBLHs are generally lower in the mid-morning and noon in the NLI than the NYC urban area whereas the ground-level O_3 are much higher in the NLI area than the urban area. However, the total O_3 in the PBL defined as the O_3 concentration multiplied PBLH indicate similar values at noon in the NYC urban and NLI coastal site on July 28-29, 2019.

Coincident high-levels of O_3, CO, NO_x, HCHO, CH_4, aerosols and BC were observed in the PBL in the NLI area; they show horizontal in-homogeneity at lower altitude (150-360 m AGL) in LIS area, this is further indicated from the satellite TROPOMI-measured tropospheric column NO_2 and HCHO. In addition, light-moderate levels of the transported wildfire smoke were indicated in the PBL from the lidar/ceilometer observations, satellite CALIPSO, NOAA-HMS fire and smoke product, and HRRR-smoke model prediction in NYC and LIS area. Overall, high O_3 levels in the NLI may be attributed to the complex impacts of the urban plumes transport, lower PBLH and land-sea breezes. This study does not discuss the chemical production and deposition process of O_3 that may also affect spatial patterns of O_3 in the coastal area, which is out of the scope of this paper.

In comparison to the observations, both the NOAA NAM-CMAQ and WRF-Chem models show good consistency of ground O_3 and PBLH at the NYC urban site. But in the North-shore of Long Island (NLI), the NOAA NAM-CMAQ model forecast (12-km grid) illustrates a timing delay of 2-3-hr for the maximum O_3 while the WRF-Chem predictions (1.3-km grid) show good consistency for the maximum O_3 timing. The NAM-CMAQ model indicates that the PBLH grows later in the morning and is lower at

noon than the observations. Further sensitivity analysis of the model simulations are highly needed with different spatial resolutions, emissions and meteorological initiation at the coastal area in the future.

Acknowledgements. This study is in part supported by the New York State Energy Research Development Authority (NYSERDA) (grant #183869) and the NOAA EPP MSI Cooperative Science Center for Earth System Science and Remote Sensing Technologies (NOAA-CESSRST II) under the Cooperative Agreement Grant # NA22SEC4810016. UMD was supported by NESCAUM, National Fish and Wildlife Foundation, NIST, NOAA/ARL, and MDE. This research is made possible by the New York State (NYS) Mesonet, original funding for the NYS Mesonet was provided by Federal Emergency Management Agency grant FEMA-4085-DR-NY, with the continued support of the NYS Division of Homeland Security & Emergency Services; the state of New York; the Research Foundation for the State University of New York (SUNY); the University at Albany, SUNY; the Atmospheric Sciences Research Center (ASRC) at SUNY Albany; and the Department of Atmospheric and Environmental Sciences (DAES) at SUNY Albany. Authors appreciate the data from NYSDEC, NOAA and NASA. The funding agencies have not reviewed the manuscript, so the views or opinions expressed herein are those of the authors and do not necessarily reflect the views or policies of these agencies. We gratefully acknowledge the valuable comments from two anonymous reviewers.

References

Abdi-Oskouei, M., Carmichael, G., Christiansen, M., Ferrada, G., Roozitalab, B., Sobhani, N., Wade, K., Czarnetzki, A., Pierce, R. B., Wagner, T., Stanier, C, 2020. Sensitivity of meteorological skill to selection of WRF-Chem physical parameterizations and impact on ozone prediction during the Lake Michigan Ozone Study (LMOS). J Geophy. Res. (Atmos.), 125 (5), e2019JD031971, https://doi.org/10.1029/2019JD031971.

Angevine, W., White, A. B., Senff, C.J., Trainer, M., Banta, R.M., Ayoub, M.A. 2003. Urban-rural contrasts in mixing height and cloudiness over Nashville in 1999. J. Geophys. Res., 108 (D3) 4092, doi: 10.1029/2001/JD001061.

Angevine, M. W., Zagar, M., Tucker, S. C., Fairall, C. W., Bariteau, L., Wolfe, D. E., Brewer, W. A. 2008. Modeling the boundary layer over Galveston Bay and the Gulf of Mexico for air pollution studies, 18th Symposium on Boundary Layers and Turbulence, 16A.1.

Bao, S., Pietrafesa, L., Gayes, P., Noble, S., Viner, B., Qian, J.-H., et al. (2023). Mapping the spatial footprint of sea breeze winds in the southeastern United States. J. Geophy. Res.: Atmos., 128, e2022JD037524. https://doi.org/10.1029/2022JD037524

Brotzge, J. A., Wang, J., Thorncroft, C. D., Joseph, E., Bain, N., Bassill, N., Farruggio, N., Freedman, J. M., Hemker, K., Jr., Johnston, D., Kane, E., McKim, S., Miller, S. D., Minder, J. R., Naple, P., Perez, S., Schwab, J. J., Schwab, M. J., Sicker, J. 2020. A Technical Overview of the New York State Mesonet Standard Network, Journal of Atmospheric and Oceanic Technology, 37(10), 1827-1845, https://doi.org/10.1175/JTECH-D-19-0220.

Caicedo, V., Rappenglueck, B., Cuchiara, G., Flynn, J., Ferrare, R., Scarino, A.J., Berkoff, T., Senff, C., Langford, A., Lefer, B., 2019. Bay-breeze and sea breeze circulation impacts on the planetary boundary layer and air quality from an observed and modeled DISCOVER-AQ Texas case study. J. Geophys. Res.: Atmosphere 124, 7359–7378. https://doi.org/10.1029/2019JD030523.

Caicedo, V., Delgado, R., Sakai, R., Knepp, T., Williams, D., Cavender, K., Lefer, B., Szykman, J., 2020. An Automated Common Algorithm for Planetary Boundary Layer Retrievals Using Aerosol Lidars in Support of the U.S. EPA Photochemical Assessment Monitoring Stations Program, J. Atmos. Oceanic Technol., 37(10), 1847-1864.

Caicedo, V, Delgado, R., Luke, W., Ren, X., Kelley, P., Stratton, P., Dickerson, R., Berkoff, T., Gronoff, G., 2021. Observations of bay-breeze and ozone events over a marine site during the OWLETS-2 campaign, Atmos. Environ. 263, 118669, https://doi.org/10.1016/j.atmosenv.2021.118669

Campbell, P. C., Tang, Y., Lee, P., Baker, B., Tong, D., Saylor, R., Stein, A., Huang, J., Huang, H.-C., Strobach, E., McQueen, J., Pan, L., Stajner, I., Sims, J., Tirado-Delgado, J., Jung, Y., Yang, F., Spero, T. L., Gilliam, R. C., 2022. Development and evaluation of an advanced National Air Quality Forecasting Capability using the NOAA Global Forecast System version 16, Geosci. Model Dev., 15, 3281–3313, https://doi.org/10.5194/gmd-15-3281-2022.

Castellanos, P., Marufu, L. T., Doddridge, B. G., Taubman, B. F., Ehrman, S. H., Dickerson, R. R., 2011, Ozone, nitrogen oxides, and carbon monoxide during pollution events over the eastern US: An evaluation of emissions and vertical mixing, J. Geophys. Res., 116, D16307, doi:10.1029/2010JD014540.

Coggon, M. M., Gkatzelis, G. I., McDonald, B. C., Gilman, J. B., et al., 2021. Volatile Chemical Product Emissions Enhance Ozone and Modulate Urban Chemistry. Proc. Natl. Acad. Sci., 118, e2026653118.

Couillard, M. H., Schwab, M. J., Schwab, J. J., Lu, C.-H., Joseph, E., Stutsrim, B., 2021. Vertical profiles of ozone concentrations in the lower troposphere downwind of New York City during LISTOS 2018–2019. J. Geophy. Res. (Atmos.), 126, e2021JD035108. https://doi.org/10.1029/2021JD035108.

Crawford, J. H., C. Warneke, J.P. Schwarz. 2021. MASTER: FIREX-AQ Airborne Campaign, Western-Central USA, Summer 2019. ORNL DAAC, Oak Ridge, Tennessee, USA. https://doi.org/10.3334/ORNLDAAC/1941

Dai, C., Wang, Q., Kalogiros, J.A., Lenschow, D. H., Zhou, M., 2014. Determining Boundary-Layer Height from Aircraft Measurements. Boundary Layer Meteorol. 152, 277–302, https://doi.org/10.1007/s10546-014-9929-z

Day, B. M., Rappenglück, B., Clements, C.B., Tucker, S. C., Brewer, A., 2010. Nocturnal boundary layer characteristics and land breeze development in Houston, Texas during TexAQS II. Atmos. Environ., 44(33), 4014–4023. https://doi.org/10.1016/j.atmosenv.2009.01.031.

Dreessen, J., Sullivan, J., Delgado, R., 2016. Observations and impacts of transported Canadian wildfire smoke on ozone and aerosol air quality in the Maryland region on June 9–12, 2015, J. Air & Waste Management Assoc., 66:9, 842-862.

Finardi, S., Agrillo, G., Baraldi, R., Calori, G., Carlucci, P., Ciccioli, P., D'Allura, A., Gasbarra, D., Gioli, B., Magliulo, V., Radice, P., Toscano, P., Zaldei, A. 2018. Atmospheric Dynamics and Ozone Cycle during Sea Breeze in a Mediterranean Complex Urbanized Coastal Site, Journal of Applied Meteorology and Climatology, 57(5), 1083-1099.

Foley, K. M., Roselle, S. J., Appel, K. W., Bhave, P. V., Pleim, J. E., Otte, T. L., Mathur, R., Sarwar, G., Young, J. O., Gilliam, R. C., Nolte, C. G., Kelly, J. T., Gilliland, A. B., Bash, J. O., 2010. Incremental testing of the Community Multiscale Air Quality (CMAQ) modeling system version 4.7, Geosci. Model Dev., 3, 205-226.

Gan, C., Wu, Y., Madhavan, B., Gross, B., Moshary, F., 2011. Application of active optical sensors to probe the vertical structure of the urban boundary layer and assess anomalies in air quality model PM2.5 forecasts, Atmos. Environ., 45 (37), 6613-6621.

Griffin, D., Zhao, X., McLinden, C. A., Boersma, F., et al., 2019. High‐Resolution Mapping of Nitrogen Dioxide with TROPOMI: First Results and Validation over the Canadian Oil Sands. Geophy. Res. Lett., 46(2): 1049–1060.

Haeffelin, M., Angelini, F., Morille, Y., Martucci, G., Frey, S., Gobbi, G.P., Lolli, S., O'Dowd, C.D., Sauvage, L., Xueref-Remy, I., Wastine, B., Feist, D.G. 2012. Evaluation of mixing-height retrievals

from automated profiling lidars and ceilometers in view of future integrated networks in Europe. Boundary-Layer Meteorol. 143, 49–75.

Haman, C. L., Couzo, E., Flynn, J. H., Vizuete, W., Heffron, B., Lefer, B. L. 2014. Relationship between boundary layer heights and growth rates with ground-level ozone in Houston, Texas, J. Geophys. Res. Atmos., 119, 6230–6245, doi: 10.1002/2013JD020473.

Han, Z. S., González-Cruz, J. E., Liu, H. N., Melecio-Vázquez, D., Gamarro, H., Wu, Y., Moshary, F., Bornstein, R. 2022. Observed sea breeze life cycle in and around NYC impacts on PBL and surface UHI and ozone patterns, Urban Climate, 42, 101109, doi.org/10.1016/j.uclim.2022.101109

Huang, J., J. McQueen, J. Wilczak, I. Djalalova, I. Stajner, P. Shafran, D. Allured, P. Lee, L. Pan, D. Tong, H. Huang, G. DiMego, S. Upadhayay, L. Monache, 2017. Improving NOAA NAQFC $PM_{2.5}$ predictions with a bias correction approach, Wea. and Forecasting, 32, 407-421.

June, N. A., Hodshire, A. L., Wiggins, E. B., et al., 2022: Aerosol size distribution changes in FIREX-AQ biomass burning plumes: the impact of plume concentration on coagulation and OA condensation/evaporation, Atmos. Chem. Phys., 22, 12803–12825.

Karambelas, A., 2020. LISTOS: Toward a Better Understanding of New York City's Ozone Pollution Problem (An overview of the Long Island Sound Tropospheric Ozone Study). EM A&WMA, https://www.awma.org/content.asp?admin=Y&contentid=657

Kelly, J. T., Bhave, P. V., Nolte, C. G., Shankar, U., Foley, K. M. 2009. Simulating emission and chemical evolution of coarse sea-salt particles in the Community Multiscale Air Quality (CMAQ) model. Geosci. Model Dev., 2, 1335–1374.

Lee, P., J. McQueen, I. Stajner, J. Huang, L. Pan, D. Tong, H. Kim, Y. Tang, Kondragunta S., M. Ruminski, S. Lu, E. Rogers, R. Saylor, P. Shafran, H. Huang, J. Gorline, S. Upadhayay, R. Artz, 2017. NAQFC developmental forecast guidance for fine particulate matter (PM2.5). Wea. and Forecasting. 32 (1): 343–360.

Li, D., Wu, Y., Gross, B., Moshary, F., 2021. Capabilities of an Automatic Lidar Ceilometer to Retrieve Aerosol Characteristics within the Planetary Boundary Layer. Remote Sens., 13, 3626. https://doi.org/10.3390/rs13183626

Li, D., Wu, Y., Gross, B., Moshary, F., 2022. Dynamics of Mixing Layer Height and Homogeneity from Ceilometer-Measured Aerosol Profiles and Correlation to Ground Level PM2.5 in New York City. Remote Sens. 14, 6370. https://doi.org/10.3390/rs14246370

Liu, T., Panday, F.M., Caine, M.C., Kelp, M., Pendergrass, D.C., Mickley, L., 2023. Is the smoke aloft? Caveats regarding the use of the Hazard Mapping System (HMS) smoke product as a proxy for surface smoke presence across the United States. Int. J Wildland Fire, https://doi.org/10.31223/X51963

Miller, P. J., 2017. Retrospective and Future Analysis of Air Quality In and Downwind of New York City, DRAFT White Paper, available at www.nescaum.org/documents/listos.

Ren, X., Salmon, O. E., Hansford, J. R., et al., 2018. Methane Emissions from the Baltimore-Washington Area Based on Airborne Observations: Comparison to Emissions Inventories, J. Geophys. Res. (Atmos.), 123, 8869–8882.

Ren, X., Hall, D. L., Vinciguerra, T., Benish, S. E., Stratton, P. R., et al., 2019. Methane emissions from the Marcellus Shale in southwestern Pennsylvania and northern West Virginia Based on Airborne Measurements, J. Geophys. Res. Atmos., 124, 1862–1878.

Ring, A., Dickerson, R. R., Sebol, A., Ren, X., Benish, S., Salawitch, R., Galasyn, A., Miller, P., Canty, T., 2023. Anthropogenic VOCs in the Long Island Sound, NY Airshed and their role in ozone production, Atmos. Environ., 296, 119583, https://doi.org/10.1016/j.atmosenv.2023.119583.

Ruminski, M., Kondragunta, S., Draxler, R., Zeng, J., 2006. Recent Changes to the Hazard Mapping System, 15th International Emission Inventory Conference, Reinventing Inventories - New Ideas in New Orleans*,* New Orleans, May 15 - 18, 2006.

Schween, J. H., Hirsikko, A., Lohnert, U., Crewell, S., 2014. Mixing-layer height retrieval with ceilometer and Doppler lidar from case studies to long-term assessment. Atmos. Meas. Tech. 7, 3685–3704.

Seidel, D. J., Ao, C. O., Li, K. 2010. Estimating climatological planetary boundary layer heights from radiosonde observations: Comparison of methods and uncertainty analysis, J. Geophys. Res., 115, D16113, doi: 10.1029/2009JD013680.

Shrestha, B., Brotzge, J. A., Wang, J., Bain, N., Thorncroft, C. D., Joseph, E., Freedman, J., Perez, S. 2021. Overview and Applications of the New York State Mesonet Profiler Network, J. Appl. Meteorol. Climat. https://journals.ametsoc.org/view/journals/apme/aop/JAMC-D-21-0104.1/JAMC-D-21-0104.1.xml

Stauffer, R. M., Thompson, A. M., Martins, D. K., Clark, R. D., Goldberg, D. L., Loughner, C. P., Delgado, R., Dickerson, R. R., Stehr, J. W., Tzortziou, M. A., 2015. Bay breeze influence on surface ozone at Edgewood, MD during July 2011. J. Atmos. Chem., *72*(3-4), 335–353.

Stein, A., Draxler, R., Rolph, G., Stunder, B., Cohen, M., Ngan, F. 2015. NOAA's HYSPLIT atmospheric transport and dispersion modeling system. Bulletin of the American Meteorological Society. 96 (12) 2059-2077. doi: 10.1175/BAMS-D-14- 00110.1.

Stull, R.B., 1988. An Introduction to Boundary Layer Meteorology. Kluwer Academic Publishers, pp. 12–16.

Sullivan, J. T., Berkoff, T., Gronoff, G., Knepp, T., et al. 2019. The Ozone Water–Land Environmental Transition Study: An Innovative Strategy for Understanding Chesapeake Bay Pollution Events, Bulletin of the American Meteorological Society*,* 100(2), 291-306.

Tao, Madankui, Arlene M. Fiore, Xiaomeng Jin, Luke D. Schiferl, Róisín Commane, Laura M. Judd, Scott Janz, John T. Sullivan, Paul J. Miller, Alexandra Karambelas, Sharon Davis, Maria Tzortziou, Lukas Valin, Andrew Whitehill, Kevin Civerolo, Yuhong Tian, 2022. Investigating Changes in Ozone Formation Chemistry during Summertime Pollution Events over the Northeastern United States**,** Environ. Sci. Technol., 56 (22), 15312-15327, DOI: 10.1021/acs.est.2c02972

Torres-Vazquez, A., Pleim, J., Gilliam, R., Pouliot, G., 2022. Performance Evaluation of the Meteorology and Air Quality Conditions from Multiscale WRF-CMAQ Simulations for the Long Island Sound Tropospheric Ozone Study (LISTOS). J. Geophy. Res.: Atmospheres, 127(5):e2021JD035890, https://doi.org/10.1029/2021JD035890.

Tucker, S.C., Senff, C.J., Weickmann, A.M., Brewer, W.A., Banta, R.M., Berg, S.P., Law, D. C., Hardesty, R.M., 2009. Doppler idar estimation of mixing height using turbulence, shear, and aerosol profiles. J. Atmos. Ocean. Technol. 26, 673–688.

Taubman, B. F., Marufu, L. T., Piety, C. A., Doddridge, B. G., Stehr, J. W., Dickerson, R. R. 2004. Airborne characterization of the chemical, optical, and meteorological properties, and origins of a combined ozone-haze episode over the eastern United States, J. Atmos. Sci., 61, 1781-1793.

Vermeuel, M. P., Novak, G. A., Alwe, H. D., Hughes, D. D., et al., 2019. Sensitivity of ozone production to NOx and VOC along the Lake Michigan coastline. J. Geophys. Res. (Atmos.), 124 (20), 10989-11006.

Winker, D. M., M. A. Vaughan, A. Omar, Y. Hu, and K. A. Powell, Z. Liu W. H. Hunt, S. A. Young, 2009. Overview of the CALIPSO Mission and CALIOP Data Processing Algorithms, J. Atmos. Oceanic Technol., 26, 2310–2323.

Wu, Y., Chaw, S., Gross, B., Moshary, F., Ahmed, S., 2009. Low and optically thin cloud measurements using a Raman-Mie lidar, Appl. Opt. 48, 1218-1227.

Wu, Y., L. Cordero, B. Gross, Moshary, F., Ahmed, S. 2012. Smoke plume optical properties and transport observed by a multi-wavelength lidar, sunphotometer and satellite, Atmos. Environ., 63, 32–42.

Wu, Y., Zhao, K., Huang, J., Arend, M., Gross, B., Moshary, F. 2019. Observation of heat wave effects on the urban air quality and PBL in New York City area, Atmos. Environ, 117024, DOI: 10.1016/j.atmosenv.2019.117024.

Wu, Y., Nehrir, A., Ren, X., Dickerson, R. R., Huang, J., et al., 2021. Synergistic aircraft and ground observations of transported wildfire smoke and its impact on air quality in New York City during the summer 2018. Sci. Total Environment. 773, 145030. https://doi.org/10.1016/j.scitotenv.2021.145030

Zhang, J., Ninneman, M., Joseph, E., Schwab, M. J., Shrestha, B., Schwab, J. J. 2020. Mobile laboratory measurements of high surface ozone levels and spatial heterogeneity during LISTOS 2018: evidence for sea breeze influence. J. Geophys. Res. (Atmos.) 125 (11), 1–19.Zhang, D., Comstock, J., Morris, V. 2022. Comparison of planetary boundary layer height from ceilometer with ARM radiosonde data, Atmos. Meas. Tech., 15, 4735–4749, https://doi.org/10.5194/amt-15-4735-2022.

Zhao, K., Bao, Y., Huang, J., Wu, Y., Arend, M., Moshary, F., 2019. A high-resolution modeling study of a heat wave-driven ozone exceedance event in New York City and surrounding regions, Atmos. Environ., 199, 368–379.

Zhao, K., Wu, Y., Huang, J., Gronoff, G., Berkoff, T., Arend, M., Moshary, F., 2023. Identification of the roles of urban plume and local chemical production in ozone episodes observed in Long Island Sound during LISTOS 2018: implications for ozone control strategies, Environment International, 174, 107887, https://doi.org/10.1016/j.envint.2023.107887.

Figures and Table Captions

Table-1. Ground site location and the data used in this study.

Table-2. PBLH comparison among the methods from ceilometer, wind lidar and virtual potential temperature (θ_v) at the North-shore of Long Island (UTC-4=local time or EDT)

Fig.1. Ground sites used in this study (See Table-1 for their coordinates and observations).
Fig. 2. Temporal variation of (a) near-surface O_3 and (b) NO_2 in the NYC urban and coastal area in Long Island during July 25-31, 2019; (c)-(d) Daily O_3-AQI on July 28 and 29, 2019 from AirNow. FP-Flax Pond, QC-Queens College, see Fig.1 and Table-1 for the site full names and locations.

Fig. 3. (a)-(b) Air temperature and RH at CCNY (1-min ave.), Stony Brook (SBK in NLI) and Fire Island (FI in SLI), (c) Wind rose at 6:00-18:00 EDT on July 25-26 and (d) July 28-30 at CCNY.

Fig.4. Comparison of MLH measured from the methods of (a) Ceilometer, (b) Wind lidar, (c–f) Virtual potential temperature (θ_v) and water vapor (H_2O) profiles at the North-shore of Long Island on July 29, 2019. (Vertical dash lines in Fig. (a): ozonesonde launch time; horizontal dash lines in (c-f): PBLH)

Fig.5. Vertical profiles of (a) aerosol total scattering coefficient (σ_{as}) at λ=550-nm, (b) virtual potential temperature (θ_v), and (c) water vapor (H_2O) measured from the UMD research aircraft near Flax Pond at 19:32-19:52 UTC on July 29, 2019. (Horizontal dash lines – PBLH estimate from each method)

Fig. 6. Ceilometer-measured backscatter intensity and MLH at (a) CCNY, (b) Eatons Neck, and (c) Fire Island during July 26-31, 2019. (MLH:mixing-layer-height; Cldz:cloud base; ALH: aerosol-layer-height)

Fig. 7. Comparison and correlation of MLH (30-min ave.) between the ceilometer and wind-lidar methods in the NYC urban (a-b), and the NLI coastal area (c-d), respectively.

Fig. 8. Diurnal variation of ground O_3 (a), MLH (b), and (c) Ratio of vertical velocity variance from the wind lidar measurements in the NYC urban and the coastal area in North-shore of Long Island (NLH) on July 28-30, 2019 (red circles: MLH in the urban area).

Fig.9. (a) Wind lidar measured carrier-noise-ratio (CNR), (b) horizontal wind speed, (c) wind direction, (d) vertical wind velocity (+up, –down) at Bronx (NYC urban) during July 28-31, 2019.

Fig.10. Same as Fig.9 except at Stony Brook (SBK) in the Northern Long Island.

Fig.11. (a) Vertical distribution of O_3, (b) wind speed (Spd) and direction (Dir.) measured from the ozonesonde at Flax Pond at 14:29-14:40 UTC on July 29, 2019 (vertical dash: wind direction at 270º).

Fig. 12. (a)-(b) Same as Fig.11 except at 19:14-19:22 UTC on July 29, 2019 (afternoon).

Fig.13. (a) Aircraft flight track and time-height for the two vertical profile measurements (P1- ascent in green; P2- descent in red), (b)-(g) Profiles of O_3, CO, aerosol scattering coefficient (horizontal dash-PBLH), NO_x, CH_4, HCHO on July 29, 2019. P1: 19:32-19:52UTC near Flax Pond; P2: 19:52-20:15UTC cross LIS.

Fig.14. (a)-(d). Tropospheric column content of NO_2 and HCHO measured from S5P/TROPOMI/ on July 28 (a, b) and 30 (c, d), 2019

Fig.15 (a)-(b) Comparisons of ground-level hourly O_3 between the WRF-Chem, NAM-CMAQ model and the observations, (c) MLH comparison in the coastal area of Long Island during July 28-30, 2019.